

See discussions, stats, and author profiles for this publication at: <http://www.researchgate.net/publication/228980439>

Mineral-specific chemical weathering rates over millennial timescales: Measurements at Rio Icacos, Puerto Rico

ARTICLE in CHEMICAL GEOLOGY · OCTOBER 2010

Impact Factor: 3.48 · DOI: 10.1016/j.chemgeo.2010.07.013

CITATIONS

18

DOWNLOADS

14

VIEWS

102

4 AUTHORS, INCLUDING:



James W. Kirchner

ETH Zurich

195 PUBLICATIONS 6,572 CITATIONS

[SEE PROFILE](#)



R. Finkel

University of California, Berkeley

441 PUBLICATIONS 11,241 CITATIONS

[SEE PROFILE](#)



Mineral-specific chemical weathering rates over millennial timescales: Measurements at Rio Icacos, Puerto Rico

Ken L. Ferrier ^{a,*}, James W. Kirchner ^{b,c,d}, Clifford S. Riebe ^e, Robert C. Finkel ^{b,f}

^a Department of Earth, Atmospheric, and Planetary Sciences, Massachusetts Institute of Technology, United States

^b Department of Earth and Planetary Science, University of California, Berkeley, United States

^c Swiss Federal Institute for Forest, Snow, and Landscape Research (WSL), Birmensdorf, Switzerland

^d Department of Environmental Sciences, Swiss Federal Institute of Technology (ETH), Zürich, Switzerland

^e Department of Geology and Geophysics, University of Wyoming, United States

^f Le Centre Européen de Recherche et d'Enseignement des Géosciences de l'Environnement (CEREGE), Aix-en-Provence, France

ARTICLE INFO

Article history:

Received 29 January 2010

Received in revised form 22 July 2010

Accepted 26 July 2010

Editor: J.D. Blum

Keywords:

Chemical weathering

Mineral weathering

Cosmogenic nuclides

Rio Icacos

Puerto Rico

ABSTRACT

Mineral weathering plays a prominent role in many biogeochemical and geomorphological processes. It supplies nutrients to soils and streams, accelerates physical erosion by weakening bedrock and producing easily erodible soil, and modulates Earth's long-term climate by drawing down atmospheric carbon dioxide. We calculate mineral-specific chemical weathering rates at two field sites in the Rio Icacos catchment, Puerto Rico, by combining new mineral abundance measurements from quantitative powder X-ray diffraction (XRD) with existing measurements of (i) soil production rates from cosmogenic nuclides, (ii) chemical alteration of the regolith from X-ray fluorescence (XRF), and (iii) dust deposition rates. The central purpose of this paper is to show that combining measurements of cosmogenic nuclides with XRF-based geochemistry and XRD-based mineralogy can, in favorable cases, provide weathering rates of abundant, soluble mineral phases in actively eroding terrain to an accuracy of better than 20% of the mean, even in places with high dust deposition rates. Mineral weathering at our two field sites is dominated by plagioclase, at rates of $3274 \pm 575 \text{ mol ha}^{-1} \text{ yr}^{-1}$ and $3077 \pm 541 \text{ mol ha}^{-1} \text{ yr}^{-1}$, followed by hornblende, at $187 \pm 71 \text{ mol ha}^{-1} \text{ yr}^{-1}$ and $308 \pm 93 \text{ mol ha}^{-1} \text{ yr}^{-1}$. Within the uncertainty of our data, all weathering of these primary minerals occurs below the saprolite-soil interface. Our measurements imply that kaolinite production in saprolite is roughly 1.3 times faster than kaolinite weathering in the soil. Our results are the first to show that field measurements of cosmogenic nuclides, XRF, XRD, and dust fluxes can be combined within the geochemical mass balance method to quantify long-term mineral weathering rates, even in locations with high dust deposition rates. This implies that the mass balance method can be a valuable tool for quantifying the effects of climate, vegetation, tectonics, and other factors on weathering rates of individual mineral phases.

© 2010 Elsevier B.V. All rights reserved.

1. Introduction

Plants, animals, and landforms are all influenced by mineral weathering. As primary minerals dissolve, they provide the nutritional foundation for terrestrial biogeochemistry by releasing solutes to natural waters and promoting secondary mineral precipitation. As bedrock is weathered to soil, it loses much of its shear strength and thus its resistance to physical erosion, leading to important differences in rates and processes of erosion in soil-mantled and bedrock landscapes. To the extent that silicate dissolution rates increase with temperature, silicate weathering regulates Earth's long-term surface temperature via the greenhouse effect, because silicate chemical weathering is the dominant sink for atmospheric CO₂ over million-year timescales (Walker et al., 1981; Berner et al., 1983). Thus,

predicting the responses of landscapes, biota, and atmospheric CO₂ concentrations to changes in environmental factors such as temperature, precipitation, and pH requires measuring how these factors influence mineral weathering rates over the long timescales of mineral weathering in the field.

A number of techniques have been used to measure mineral weathering rates. Dissolution rates have often been measured in laboratory experiments (e.g., Chou and Wollast, 1984; Swoboda-Colberg and Drever, 1993; Anbeek et al., 1994), but these lab-derived rates are typically several orders of magnitude faster than field-derived rates (White and Brantley, 2003, and references therein), reflecting differences between the lab and the field in both the weathering environment (e.g., in deviations of the pore fluid from thermodynamic saturation) and in the mineral surfaces themselves (e.g., in mineral surface area, density of structural heterogeneities, and leached layers and clay coatings that build up over time). In field settings, chemical erosion rates of individual mineral phases were first inferred by ascribing solute fluxes of particular elements (e.g.,

* Corresponding author.

E-mail address: kferrier@mit.edu (K.L. Ferrier).

sodium) to dissolution of particular minerals (e.g., albite). This approach, pioneered in Garrels and Mackenzie (1967), has since been extended to rationalize a suite of solute fluxes in terms of a suite of mineral weathering rates, and has been applied at a number of catchments (e.g., Cleaves et al., 1970; Paces, 1983; Velbel, 1985; Clayton, 1986; Taylor and Velbel, 1991; Swoboda-Colberg and Drever, 1993; Clow and Drever, 1996; Price et al., 2005). Inferring mineral weathering rates with this catchment-scale solute mass balance method requires measuring the export of solutes from the catchment in stream water, the import of solutes by atmospheric deposition, and any changes in solute storage within the catchment. These additional sources and sinks of solutes can be significant fractions of the outgoing solute fluxes and can have large uncertainties, which may confound interpretations of catchment-scale mineral dissolution rates (e.g., Taylor and Velbel, 1991). At the finer scale of a weathering profile, mineral weathering rates may also be inferred from gradients in vertical solute fluxes within the soil and saprolite (Murphy et al., 1998; White, 2002, 2003; White et al., 2005, 2008). Following conventional definitions, in this paper we use the term “bedrock” to refer to unaltered parent material, “saprolite” to refer to weathered bedrock which retains the original structure and fabric of unaltered rock, and “soil” to refer to the layer where parent material has been physically and/or chemically disrupted by biotic and/or abiotic processes. Together, the saprolite and soil comprise the regolith.

In this paper we measure field-derived mineral weathering rates by combining concentrations of minerals and immobile elements in the bedrock and the regolith with measurements of soil production rates, under the assumption that the composition and mass per unit area of the regolith are in steady state. Classified as a solid-phase mass balance method because it relies on measurements of the bulk chemistry and mineralogy of regolith and bedrock, this approach has appeared in several different formulations in the literature. The approach we use to calculate mineral weathering rates in this paper is an extension of the mass balance formulation in Stallard (1985). A key advantage of the solid-phase mass balance approach over solute-based approaches is that it is based on regolith composition rather than solute composition, and thus yields mineral weathering rates averaged over the long timescales of regolith development (typically 10^3 – 10^5 years) rather than over the short timescales of solute transport through the weathering profile or catchment (typically <10 years). After presenting the mathematical framework for this approach in Section 2, we apply this method to two sites in the Rio Icacos catchment, Puerto Rico, in Section 5. This application uses previously reported concentrations of immobile elements and cosmogenic ^{10}Be (Riebe et al., 2003) and new measurements of mineral abundances in the same rock, soil, and saprolite samples analyzed in Riebe et al. (2003).

2. A steady state framework for measuring mineral-specific chemical weathering rates in saprolite and soil

Chemical weathering rates can be determined by combining measurements of chemical mass loss (inferred from immobile element enrichment in regolith relative to bedrock) with an appropriate rate constant derived from, e.g., the age of the soil in non-eroding landscapes (Merritts et al., 1991), or the overall flux of material from the regolith (Stallard, 1985) measured with cosmogenic nuclides (White et al., 1998; Riebe et al., 2001a). Here we review the theoretical underpinnings for this technique. The mathematical framework is an extension of a formulation proposed by Stallard (1985), and it follows Yoo and Mudd (2008) and Owen et al. (2008) in its inclusion of dust deposition in the mass balance and it follows Dixon et al. (2009) in its application to both saprolite and soil. An important advantage of this steady state framework is that it is applicable to actively eroding terrain, and thus is not restricted to non-eroding weathering profiles of known age, as classical chronosequence studies are (e.g., Merritts et al., 1991). It also extends the

model by explicitly demonstrating how mineral-specific weathering rates may be calculated in saprolite and soil.

Before outlining the mass balance framework, we first define a few terms, since terminology can be variable across disciplines that study weathering. In this paper we use the term “chemical weathering” to refer exclusively to chemical alteration of minerals. This process is distinct from “chemical erosion”, which we define as the export of dissolved mass from the weathering zone. This distinction is important for minerals that do not dissolve completely during chemical weathering (e.g., for plagioclase, which weathers to solutes and secondary clays); in such cases chemical erosion rates are smaller than chemical weathering rates because only a fraction of the primary mineral mass dissolves and thus can be eroded in solution. In contrast to chemical erosion, we use the term “physical erosion” to denote mass losses from the weathering zone by physical processes. The sum of physical and chemical erosion we refer to as “denudation”.

The following mass balance framework differs from those in some recent studies in that it neglects changes in soil composition during downslope transport. Some studies have found that chemical weathering of soil during downslope transport can affect regolith composition and thus affect estimates of mineral weathering rates based on regolith composition (Mudd and Furbish, 2004; Green et al., 2006; Yoo et al., 2007; Owen et al., 2008; Yoo and Mudd, 2008; Yoo et al., 2009). Other studies, however, have observed negligible downslope variation in soil composition (Dixon et al., 2009). In the present paper we do not treat the chemical weathering of soil during downslope transport for three reasons. First, the samples presented in this paper were not collected along downslope hillslope transects, and so are not able to shed light on chemical weathering during downslope transport. Second, we are unaware of measurements that demonstrate systematic downslope variations in soil composition at Rio Icacos. Lastly, because the vast majority of chemical weathering at Rio Icacos occurs near the base of the saprolite (e.g., White et al., 1998), the additional chemical weathering that occurs during downslope soil transport should be small relative to the total extent of weathering at our field sites. By neglecting this issue in the mass balance, we implicitly assume that downslope gradients in soil chemistry are negligible.

The mass balance framework begins by considering an actively eroding hillslope (Fig. 1) in which both soil and saprolite maintain a constant mass per unit area of hillslope per time. Saprolite is defined here as chemically weathered bedrock, susceptible to mass loss by chemical dissolution but not by physical erosion. We distinguish soil from saprolite by defining soil as the portion of the weathered profile that is physically mobile, and thus is susceptible to mass losses by both chemical dissolution and physical erosion. In steady state, the rate at which mass is added to the soil – i.e., the soil production rate P_{soil} plus the dust deposition rate P_d – is balanced by the rate at which mass is lost from the soil.

$$P_{\text{soil}} + P_d = E + W_{\text{soil}} \quad (1)$$

Here E and W_{soil} are the physical erosion rate and chemical erosion rate in soil, and, like P_{soil} and P_d , have dimensions of mass per unit area of hillslope per time. The flux of an individual mineral or element X into the soil is the sum of the influxes of X from the saprolite and dust, and in steady state this rate is matched by the rate at which X is lost from the soil by physical erosion and chemical erosion.

$$P_{\text{soil}}X_{\text{sap}} + P_dX_d = EX_{\text{soil}} + W_{\text{soil},X} \quad (2)$$

Here X_{sap} , X_{soil} , and X_d are the concentrations (mol M^{-1}) of X in saprolite, soil, and dust, respectively, and $W_{\text{soil},X}$ is the chemical erosion rate of X in the soil ($\text{mol L}^{-2}\text{T}^{-1}$). If X is a chemically “immobile” element or mineral – that is, if X is so resistant to

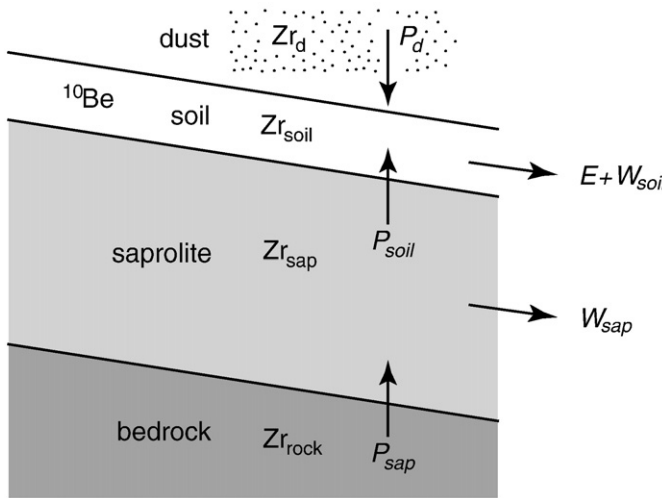


Fig. 1. Schematic of a hillslope on which a layer of soil overlies a layer of saprolite, which itself overlies unweathered bedrock. Bedrock is converted to saprolite at a rate P_{sap} , and the saprolite loses mass through chemical erosion at a rate W_{sap} and through incorporation into the soil at a rate P_{soil} . The soil gains mass from saprolite at a rate P_{soil} and from dust deposition at a rate P_d , and loses mass by chemical erosion at a rate W_{soil} as well as by physical erosion at a rate E . As described in the text, we calculate W_{sap} , W_{soil} , and E by combining measured concentrations of cosmogenic ^{10}Be in soil-borne quartz with concentrations of an immobile element (e.g., Zr) in the soil, saprolite, bedrock, and dust.

dissolution that its chemical erosion rate $W_{soil,X}$ is negligible – then Eq. (2) yields the following expression for the physical erosion rate:

$$E = P_{soil} \frac{Zr_{sap}}{Zr_{soil}} + P_d \frac{Zr_d}{Zr_{soil}}. \quad (3)$$

Here we have substituted zirconium, which occurs predominantly in zircons and which is frequently assumed to be immobile, for X . Eq. (3) can be combined with Eq. (1) to yield an expression for the soil chemical erosion rate W_{soil} .

$$W_{soil} = P_{soil} \left(1 - \frac{Zr_{sap}}{Zr_{soil}} \right) + P_d \left(1 - \frac{Zr_d}{Zr_{soil}} \right) \quad (4)$$

Similarly, substituting Eq. (3) into Eq. (2) yields an expression for the chemical weathering rate of mineral phase X in the soil.

$$W_{soil,X} = P_{soil} \left(X_{sap} - X_{soil} \frac{Zr_{sap}}{Zr_{soil}} \right) + P_d \left(X_d - X_{soil} \frac{Zr_d}{Zr_{soil}} \right) \quad (5)$$

A similar analysis to Eqs. (1)–(5) provides expressions for the same rates in saprolite. If the combined mass of saprolite and soil stays constant over time and if dust deposition does not affect saprolite composition, then the rate at which bedrock is converted to saprolite – i.e., the saprolite production rate P_{sap} – is balanced by the rate at which mass is lost from the soil and saprolite, commonly called the denudation rate.

$$P_{sap} = P_{soil} + W_{sap} \quad (6)$$

In steady state, conservation of mass for a mineral or element X implies that

$$P_{sap} X_{rock} = P_{soil} X_{sap} + W_{sap,X}. \quad (7)$$

For an immobile element like zirconium, $W_{sap,Zr}$ is negligible and Eq. (7) then yields an expression for the saprolite production rate in

terms of the soil production rate and the concentrations of zirconium in saprolite and bedrock.

$$P_{sap} = P_{soil} \frac{Zr_{sap}}{Zr_{rock}} \quad (8)$$

Substituting Eq. (8) into Eq. (6) yields the bulk chemical erosion rate in saprolite W_{sap} ,

$$W_{sap} = P_{soil} \left(\frac{Zr_{sap}}{Zr_{rock}} - 1 \right), \quad (9)$$

and substituting Eq. (8) into Eq. (7) yields the mineral-specific chemical weathering rate in saprolite $W_{sap,X}$,

$$W_{sap,X} = P_{soil} \left(X_{rock} \frac{Zr_{sap}}{Zr_{rock}} - X_{sap} \right) \quad (10)$$

If we again use the term “regolith” to mean the soil and saprolite together, then the bulk chemical erosion rate and the mineral-specific chemical weathering rates in the regolith are

$$W_{regolith} = W_{soil} + W_{sap} = P_{soil} Zr_{sap} \left(\frac{1}{Zr_{rock}} - \frac{1}{Zr_{soil}} \right) + P_d \left(1 - \frac{Zr_d}{Zr_{soil}} \right) \quad (11)$$

and

$$W_{regolith,X} = W_{soil,X} + W_{sap,X} = P_{soil} Zr_{sap} \left(\frac{X_{rock}}{Zr_{rock}} - \frac{X_{soil}}{Zr_{soil}} \right) + P_d \left(X_d - X_{soil} \frac{Zr_d}{Zr_{soil}} \right), \quad (12)$$

respectively.

At field sites that have soil and bedrock but no saprolite (or saprolite that is not substantially depleted by chemical losses), W_{sap} and $W_{sap,X}$ are zero and Eqs. (11) and (12) simplify to

$$W_{regolith} = W_{soil} = P_{soil} \left(1 - \frac{Zr_{rock}}{Zr_{soil}} \right) + P_d \left(1 - \frac{Zr_d}{Zr_{soil}} \right) \quad (13)$$

and

$$W_{regolith,X} = W_{soil,X} = P_{soil} \left(X_{rock} - X_{soil} \frac{Zr_{rock}}{Zr_{soil}} \right) + P_d \left(X_d - X_{soil} \frac{Zr_d}{Zr_{soil}} \right), \quad (14)$$

respectively (Riebe et al., 2001b, 2003, 2004a,b).

Mineral-specific chemical weathering rates in soil and saprolite can thus be estimated by measuring the soil production rate and concentrations of minerals and immobile elements in soil, saprolite, dust, and bedrock. In cases where dust influxes are negligible, all terms that include P_d become insignificant and these expressions converge to the same expressions derived in Dixon et al. (2009), as they should.

Below we use this mass balance framework to calculate mineral-specific chemical weathering rates at two sites in Rio Icacos, Puerto Rico. We do so by combining new measurements of mineral concentrations estimated with quantitative X-ray diffraction (XRD) with previous measurements of soil production rates estimated from cosmogenic ^{10}Be concentrations in soil-borne quartz (Riebe et al., 2003), immobile element concentrations in soil, saprolite, and bedrock measured with X-ray fluorescence (XRF) (Riebe et al., 2003), and dust flux and dust composition (Glaccum and Prospero, 1980; Herwitz et al., 1996; Pett-Ridge et al., 2009).

3. Field sites: Rio Icacos, Puerto Rico

We measured mineral-specific chemical weathering rates in two small tributary catchments of Rio Icacos in Puerto Rico's Luquillo Mountains (Fig. 2), in a densely vegetated tropical rainforest where the climate is hot (mean annual temperature = 22 °C; White et al., 1998) and humid (mean annual precipitation = 4200 mm yr⁻¹; McDowell and Asbury, 1994). The Rio Blanco quartz diorite that underlies the catchment is dominated by plagioclase feldspar and quartz, with lesser amounts of hornblende, biotite, and accessory potassium feldspar (Seiders, 1971; White et al., 1998). Directly above the bedrock is a narrow zone of saprock a few tens of cm thick (White et al., 1998), in which pristine rock rapidly grades to deeply weathered saprolite. Above the saprock lies an oxidized saprolite layer up to 8 m thick, and although the saprolite appears physically undisturbed its density (1.19–1.35 g cm⁻³) is less than half that of its parent rock (2.70 g cm⁻³), reflecting the near-total loss of plagioclase and hornblende (White et al., 1998). Above the saprolite is a low-density (1.19–1.37 g cm⁻³), bioturbated inceptisol 50–100 cm thick, which grades from an organic-rich A horizon in the upper 10 cm of the profile to a clay-rich B horizon at depths greater than 40 cm (White et al., 1998; Buss et al., 2005). Landsliding is common, occurring primarily in the form of shallow soil slips and debris flows, and accounts for roughly 90% of total hillslope sediment fluxes (Larsen and Simon, 1993; Larsen, 1997), while soil creep, tree throw and slope wash dominate soil transport on hillslopes that have not experienced recent landsliding (Larsen et al., 1999).

Rio Icacos has been the site of many chemical weathering studies. Measurements of solute fluxes in soils and streams at Rio Icacos have yielded bulk chemical weathering fluxes over annual to decadal timescales (McDowell and Asbury, 1994; Stonestrom et al., 1998; White et al., 1998), and long-term bulk chemical weathering rates have been calculated from the chemical and isotopic compositions of regolith relative to parent bedrock (Stonestrom et al., 1998; White et al., 1998; Riebe et al., 2003). Mineral-specific chemical weathering rates at Rio Icacos have been inferred for plagioclase feldspar (Turner et al., 2003; Buss et al., 2008), biotite (Murphy et al., 1998; White, 2002; Buss et al., 2008), hornblende (Buss et al., 2008), and quartz (Schulz and White, 1999). These studies show that silicate weathering rates at Rio Icacos are among the fastest documented on Earth.

Dust deposition plays an important role in contributing mass to the soils in Rio Icacos. A number of studies examining dust transport from northern Africa to the Caribbean have concluded that African dust is a major driver of soil development on many Caribbean islands

(e.g., Prospero et al., 1970; Glaccum and Prospero, 1980; Prospero et al., 1981; Muhs et al., 1990; Herwitz et al., 1996; Prospero and Lamb, 2003; Mahowald et al., 2006; Muhs et al., 2007). There have been no direct physical measurements of dust deposition rates in the Rio Icacos catchment, but a recent study has concluded, based on discrepancies between inputs and outputs in a Rio Icacos Sr isotope budget, that Saharan dust contributes $21 \pm 7 \text{ t km}^{-2} \text{ yr}^{-1}$ to the Rio Icacos catchment (Pett-Ridge et al., 2009), an estimate consistent with predictions of atmospheric dust transport models (Mahowald et al., 2006). Given that millennial-timescale soil production rates from saprolite are 113 ± 17 and $118 \pm 17 \text{ t km}^{-2} \text{ yr}^{-1}$ at our two Rio Icacos field sites (Riebe et al., 2003; discussed further in Section 4), a dust flux of $21 \pm 7 \text{ t km}^{-2} \text{ yr}^{-1}$ represents a non-trivial contribution to Rio Icacos soils. We are unaware of any direct measurements of dust mineralogy or Zr concentrations at Rio Icacos. However, measurements in Barbados and Miami of dust mineralogy from Saharan dust outbreaks show little variation in dust mineralogy across the Caribbean (Glaccum and Prospero, 1980), consistent with homogenization of Saharan dust during transatlantic transport (e.g., Reid et al., 2003). This suggests that Saharan dust falling in Puerto Rico, which lies between Barbados and Miami, is likely to have a composition similar to Saharan dust measured at Barbados and Miami.

4. Methods

In this study we apply the mass balance framework to two subcatchments of Rio Icacos (RI-1 and RI-4 in Fig. 2) where Riebe et al. (2003) measured cosmogenic ¹⁰Be concentrations in soil-borne quartz and Zr concentrations in soil, saprolite, and bedrock. In that study, Riebe et al. collected rock samples from surface outcrops, saprolite samples from auger cores and landslide scars, and soil samples from a variety of locations and depths within the two subcatchments. Here we present new measurements of mineral abundances in the same rock, saprolite, and soil samples that were analyzed in Riebe et al. (2003), and combine these new measurements with the existing ¹⁰Be and Zr measurements of Riebe et al. (2003), the dust flux estimates of Pett-Ridge et al. (2009), and the dust compositions of Glaccum and Prospero (1980) and Herwitz et al. (1996) to estimate new mineral weathering rates at Rio Icacos. Sample locations, depths, and hillslope gradients are listed in the Supplementary file (Table SF2, Figs. SF1 and SF2). For further details of the sample collection and the ¹⁰Be and Zr measurements we refer the reader to Riebe et al. (2003). Below we discuss the methods we used to measure mineral abundances and discuss the reasons for revising estimates of soil production rates from Riebe et al.'s (2003) ¹⁰Be measurements.

4.1. Soil production rates inferred from cosmogenic nuclides

Riebe et al. (2003) first estimated soil production rates at sites RI-1 and RI-4 (Fig. 2) by measuring concentrations of cosmogenic ¹⁰Be in soil-borne quartz. Beryllium-10 is produced in quartz only through interactions of cosmogenic high-energy neutrons and muons with atomic nuclei in the crystal lattice (e.g., Lal, 1991). Because the fluxes of these cosmogenic particles decrease exponentially below the Earth's surface, the rate of ¹⁰Be production in quartz also decreases exponentially with depth. Concentrations of ¹⁰Be in quartz collected from surface soils thus record the integrated exposure of quartz to cosmogenic radiation during its exhumation from depth. Several studies have shown that the steady state soil denudation rate may be inferred from cosmogenic nuclide concentrations in the rock underlying the soil (e.g., Heimsath et al., 1997) or, if production of cosmogenic nuclides in the soil during downslope soil transport is negligible relative to the production of cosmogenic nuclides during exhumation, in the soil itself (e.g., Brown et al., 1995; Granger et al.,

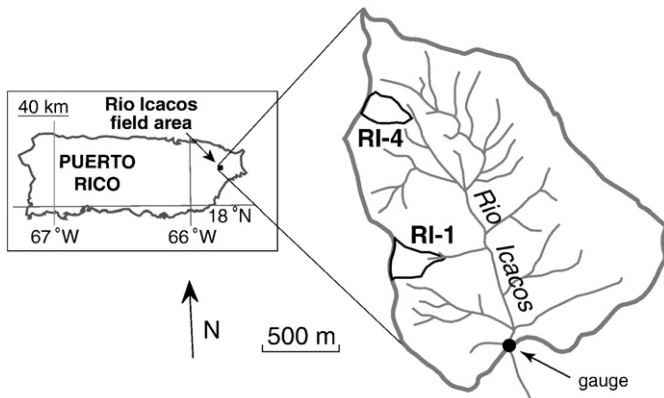


Fig. 2. Field sites within the Rio Icacos catchment, Puerto Rico. Rock and soil samples were collected in subcatchment RI-1, and rock, saprolite, and soil samples were collected in subcatchment RI-4. See Figs. SF1 and SF2 in the Supplementary file for maps of individual sample locations within each subcatchment. Subcatchment RI-1 is part of the Quebrada Guaba drainage, and also encompasses the location of the lysimeter measurements of White et al. (1998). Light gray lines denote streams, and thick gray lines denote the catchment boundary. Figure adapted from Riebe et al. (2003).

Table 1
Inputs to CRONUS denudation rate calculator, v. 2.2.^a

	RI-1	RI-4
Latitude (°N)	18.284	18.284
Longitude (°W)	65.788	65.788
Parent material density (g cm ⁻³)	1.25	1.25
Atmospheric scaling	Standard	Standard
Sample thickness (cm)	2	2
[¹⁰ Be] ($\times 10^5$ atoms g ⁻¹) ^b	1.83 ± 0.14	1.76 ± 0.10
Elevation (m) ^b	700	750
Topographic shielding ^b	0.937	0.902
¹⁰ Be standardization	KNSTD	KNSTD

^a Balco et al. (2008).

^b Riebe et al. (2003).

1996). Under the steady state assumption, the soil production rate equals the soil denudation rate.

In light of recent efforts by the cosmogenic isotope research community to standardize calculation of cosmogenic-based denudation rates (Balco et al., 2008), and because our new measurements of quartz abundances at Rio Iacacos permit calculation of a correction factor due to quartz enrichment in the soil (Small et al., 1999; Riebe et al., 2001a), here we recalculate soil production rates with the CRONUS calculator (Balco et al., 2008) rather than use the rates previously calculated for these sites by Riebe et al. (2003). The CRONUS calculator takes as inputs the relevant sample characteristics (latitude and longitude, elevation, topographic shielding, sample thickness, parent material density, and the measured ¹⁰Be concentration, for which values specific to RI-1 and RI-4 are listed in Table 1) and computes soil production rates using several different cosmogenic nuclide production scaling schemes (see Balco et al., 2008 for details). We use the Lal and Stone constant production rate scaling scheme in our analysis (Lal, 1991; Stone, 2000); other scaling schemes yield soil production rates that are faster by 3–10%. In calculating soil production rates from cosmogenic ¹⁰Be in amalgamated soil samples, we repeat Riebe et al.'s (2003) assumption that the sampled soils are well mixed. After computing rates with the CRONUS calculator, we modified these rates following Small et al. (1999) and Riebe et al. (2001a) to account for biases in ¹⁰Be concentrations due to quartz enrichment. If chemical erosion of soluble minerals leaves quartz enriched in regolith relative to its parent material, soil production rates inferred from ¹⁰Be concentrations in quartz will be biased to the extent that quartz's exposure to cosmogenic radiation is longer than that of the average mineral in the parent

material. To correct for this bias, we multiplied the CRONUS-calculated rates by a quartz enrichment factor (Small et al., 1999; Riebe et al., 2001a) of 1.68 ± 0.19 derived from our measured quartz concentrations to yield soil production rates of 113 ± 17 t km⁻² yr⁻¹ at RI-1 and 118 ± 17 t km⁻² yr⁻¹ at RI-4. These rates are 22–26% higher than those originally reported in Riebe et al. (2003). These estimates should be unaffected by the exposure of dust-borne quartz to cosmogenic radiation, because Riebe et al. (2003) measured ¹⁰Be concentrations in quartz extracted from the >250 μm size fraction of the amalgamated soil samples, a practice that excludes dust-derived quartz, which is likely composed almost entirely of particles smaller than 20 μm (Prospero et al., 1970).

These soil production rates are averaged over the timescale of ¹⁰Be accumulation in quartz, which at these sites is approximately 14 kyr. This timescale is calculated as Λ/P_{soil} , where Λ is the so-called attenuation length for ¹⁰Be production by high-energy spallation. This attenuation length is an exponential scaling constant that describes how the intensity of cosmogenic radiation is attenuated as it passes through matter, typically taken to be 160 g cm⁻² (Gosse and Phillips, 2001), which can be converted to a true length scale by dividing by the density of the material the cosmogenic radiation is passing through. In granite of density 2.7 g cm⁻³, for example, this translates to a depth of 59 cm. The value of the empirical constant Λ is based on calculations on an infinite horizontal surface (e.g., Gosse and Phillips, 2001). Soil production rates inferred from cosmogenic nuclides are thus considered to be rates of mass loss in the vertical direction (i.e., per unit area in map view), not normal to the hillslope.

We consider our measured ¹⁰Be concentrations in soil-borne quartz to be a proxy for soil production rates, and not saprolite production rates, because the thickness of soil plus saprolite at Rio Iacacos is much larger than the penetration depth of ¹⁰Be-producing cosmogenic neutrons. This implies that the great majority of cosmogenic ¹⁰Be in soil-borne quartz is produced above the saprolite–bedrock boundary, which in turn implies that ¹⁰Be concentrations in soil-borne quartz do not record the mass losses occurring by chemical erosion at the saprolite–bedrock boundary. Instead, concentrations of ¹⁰Be in soil-borne quartz at Rio Iacacos reflect the integrated exposure of quartz to cosmogenic radiation in the soil and upper saprolite, and thus reflect the rate of mass loss in the soil and upper saprolite. Because saprolite density and chemistry are nearly constant in the upper saprolite (White et al., 1998), we assume that the rate of mass loss from the upper saprolite is negligible relative to that in the soil. From this it follows that cosmogenic ¹⁰Be concentrations in soil-borne quartz are, to first-order, a reflection of the total rate of mass loss from the soil, which in steady state equals the soil production rate. The soil production rates we report for site RI-1 and RI-4 were calculated under the assumption of steady state soil formation and denudation, which at Rio Iacacos is likely a reasonable approximation (Turner et al., 2003; Fletcher et al., 2006). We then relate these P_{soil} rates to the saprolite production rate through concentrations of immobile Zr in the rock and saprolite (Eq. (8)).

Table 2
Tests of FULLPAT on prepared mineral mixtures.

	Actual abundance (%)	FULLPAT abundance (%) ^a	Absolute difference (%)
<i>Mixture 4</i>			
Quartz	60.0	61.9 ± 2.1	1.9 ± 2.1
Kaolinite	30.0	27.1 ± 0.5	2.9 ± 0.5
Goethite	10.0	13.1 ± 0.3	3.1 ± 0.3
Total	100.0	102.1 ± 2.2	
<i>Mixture 5</i>			
Andesine	35.0	36.2 ± 0.6	1.2 ± 0.6
Quartz	25.0	27.1 ± 0.4	2.1 ± 0.4
Labradorite	15.0	15.3 ± 0.9	0.3 ± 0.9
Hornblende	10.0	9.5 ± 0.2	0.5 ± 0.2
Biotite	5.6	5.2 ± 0.2	0.4 ± 0.2
Albite	5.0	4.7 ± 0.2	0.3 ± 0.2
Magnetite	4.4	5.8 ± 0.2	1.4 ± 0.2
Total	100.0	103.8 ± 1.2	

^a Because of small variations in XRD scans of any given sample when repacked and remeasured, we ran all samples four times on the XRD, repacking samples in the sample holder between each scan, and so generated four slightly different XRD patterns for each sample. The uncertainties listed here are the standard errors associated with the variability in FULLPAT-determined mineral abundances on the four XRD patterns.

4.2. Mineral abundances inferred from powder XRD patterns

We determined mineral abundances in rock, saprolite, and soil samples through quantitative analysis of X-ray diffraction (XRD) patterns measured on powdered samples. Although the principle underlying quantitative powder XRD is straightforward – the XRD pattern of a powdered sample should be the sum of the XRD patterns of the sample's constituent mineral phases, scaled by their relative abundances – in practice calculating mineral abundances from XRD patterns is limited by factors that affect measured XRD patterns (e.g., crystallite size, preferred orientation of crystallites during sample preparation, variation in mineral composition, and degree of structural disorder; e.g., Jenkins and Snyder, 1996). Because of these practical complications, uncertainties for mineral abundances determined from quantitative XRD are typically no better than 2–3%

absolute (e.g., Hillier, 2000; Chipera and Bish, 2002; Omotoso et al., 2006; Jeong et al., 2008; Eberl and Smith, 2009), implying that powder XRD may be useful for quantifying high-abundance mineral phases but has limited utility for quantifying trace mineral phases.

In our analyses we used FULLPAT (Chipera and Bish, 2002) to determine mineral abundances in our rock, saprolite, and soil samples based on each sample's powder XRD pattern. FULLPAT is an inversion method that calculates mineral abundances by creating a synthetic XRD pattern from XRD patterns of standard minerals and adjusting the abundances of the standard minerals to optimize the fit between the synthetic pattern and the measured sample pattern. Unlike some earlier quantitative XRD methods (e.g., Chung, 1974), FULLPAT does not scale the sum of all mineral abundances in a sample to 100%, and thus is able to accurately quantify the abundances of known mineral phases even if other mineral phases in the sample are unquantified. Fig. 3 shows an example of FULLPAT's approach on a test sample that we prepared from a mixture of several standard minerals.

Within FULLPAT we calculated mineral abundances in two steps. In the first step, we allowed FULLPAT to scale all mineral abundances simultaneously; this yielded a synthetic pattern that closely matched the observed sample pattern. In the second step, we refined the abundance of each mineral phase individually, allowing FULLPAT to change the abundance of only one mineral phase at a time while keeping other mineral abundances constant. This refinement step was based only on the integrated intensity of the relevant mineral's

highest-intensity peak, and was carried out while ensuring that the background intensity of the synthetic pattern matched the background intensity of the sample pattern. After refining the abundance of one mineral phase in this manner, we refined the abundances of the other minerals in the same manner.

A central requirement of this approach is that the XRD patterns of the standard minerals match the XRD patterns of the minerals present in the sample. Because some mineral phases have varying crystal structures – and hence varying XRD patterns – the best minerals to use as standards are pure mineral separates from the field samples themselves. This was our approach for quartz and plagioclase. Because of difficulties separating sufficient quantities of pure hornblende and biotite from field samples at Rio Iacisos, we used a synthetic hornblende pattern (ID# 01-089-7282) from the Powder Diffraction File (ICDD, 2003) for our hornblende standard, and a biotite from Ward's Scientific, sourced in Bancroft Mica Mine, for our biotite standard.

Does this XRD-based approach for measuring mineral abundances work? Before using FULLPAT to calculate mineral abundances in our samples from Rio Iacisos, we tested FULLPAT's accuracy on mineral mixtures that we prepared ourselves, with one mixture designed to mimic a granitic rock and another to mimic a highly weathered soil. The results of these tests are shown in Table 2 and Fig. 4. In these tests, FULLPAT-determined mineral abundances to an accuracy of 3.1% absolute (i.e., 3.1% of the total sample mass) or better, similar to the results of similar tests in Chipera and Bish (2002).

We prepared samples for XRD analysis by powdering them to a median grain size of approximately 5 μm , and adding an internal standard (1-micron corundum) to each sample in a 4:1 sample:standard ratio. These mixed powders were then packed into a back-loaded mount atop a frosted glass slide, and scanned under Co-K α radiation from 4 to 9° 2 θ on a Phillips X'Pert Pro diffractometer. We found that multiple XRD patterns of the same sample differed slightly between specimens; that is, repacking and remeasuring the same sample produced slightly different XRD patterns. This variability may be merely a consequence of the counting statistics associated with X-rays diffracted from randomly oriented crystallites (e.g., Alexander et al., 1948). To account for this variability, we measured four XRD patterns for each sample (repacked between measurements), ran FULLPAT on each of the four patterns, and report the mean calculated mineral abundance over all four runs (Table SF2, Supplementary file).

It is possible that some of the variability between XRD patterns may be due to preferred orientation of crystallites within the powder, although our tests on self-prepared mineral mixtures suggest that this effect should be small, even on the phyllosilicates that should be most susceptible to preferred orientation (Table 2, Fig. 4). Recently, other sample preparation techniques such as spray-drying (Hillier, 2000; Kleeberg et al., 2008) have been shown to be especially successful at reducing preferred orientation in powder XRD specimens. Future studies that follow the procedures of Hillier (2000) are thus likely

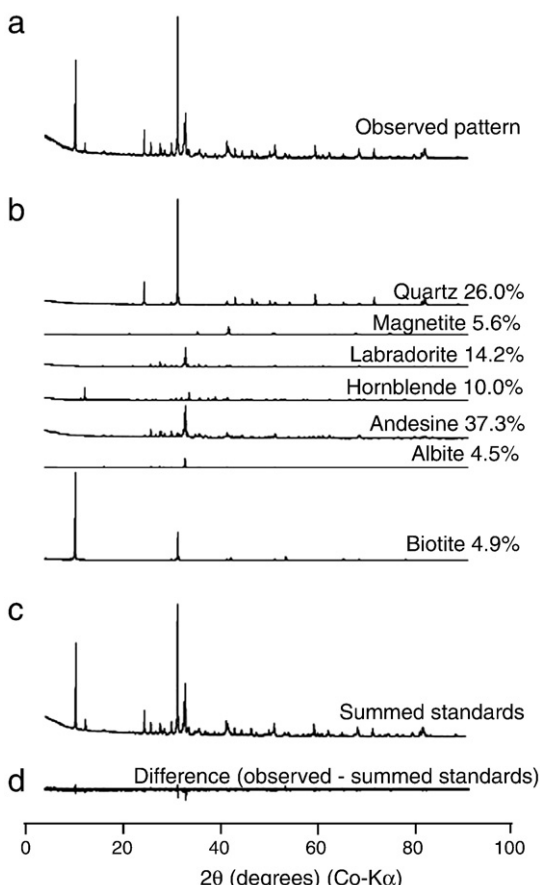


Fig. 3. FULLPAT (Chipera and Bish, 2002) calculates mineral abundances in a sample by comparing the sample's measured XRD pattern (a) to a synthetic XRD pattern (c), which is created by summing together scaled XRD patterns of standard minerals (b). The scaling factors on the standard mineral patterns are the best-fit mineral abundances, and they are scaled to minimize the difference (d) between the measured pattern and the synthetic pattern. The observed pattern here (a) is from a test sample that we prepared in the lab by combining standard minerals in known quantities, and the synthetic pattern (c) is FULLPAT's fit to the observed pattern. Figure modeled after a similar example in (Chipera and Bish, 2002).

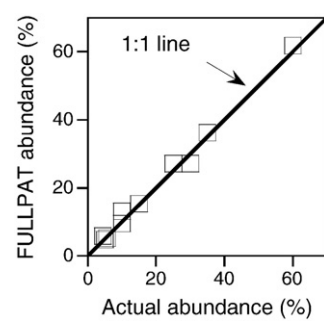


Fig. 4. Our tests of FULLPAT (Chipera and Bish, 2002) on specially prepared mineral mixtures (Table 2) verify that this XRD-based method can provide close estimates of actual mineral abundances for a variety of minerals over a wide range of abundances.

yield the most accurate estimates of mineral abundances, which in turn will yield the most accurate estimates of mineral weathering rates within the mass balance framework.

4.3. Uncertainties in inferred mineral-specific chemical weathering rates

How accurately can mineral-specific chemical weathering rates be determined with this approach? Standard error propagation shows that uncertainties in W_X derive from four sources: uncertainties in soil production rates, uncertainties in dust deposition rates, uncertainties in Zr concentrations, and uncertainties in mineral abundances. From a practical standpoint, uncertainties in Zr concentrations and dust fluxes at our field sites are negligible compared to the other uncertainties (Tables 3 and 4), so here we focus only on the errors in soil production rate and mineral abundances.

The uncertainty in soil production rate P_{soil} stems primarily from the uncertainty in the production rate P_{Be} of cosmogenic ^{10}Be (at sea level and high latitude, $P_{\text{Be}} = 5.1 \pm 0.3$ atoms of ^{10}Be per gram of quartz per year; Stone, 2000). Other uncertainties can stem from uncertainties in the degree of shielding by snow (e.g., Schildgen et al., 2005) or vegetation (e.g., Ferrier et al., 2005), analytical uncertainties in the measurement of ^{10}Be , and uncertainties in the mass attenuation constants of gamma-ray neutrons and muons (see review in Gosse and Phillips, 2001), all of which we assume are negligible at RI-1 and RI-4. Typically, the uncertainty in the ^{10}Be production rate dwarfs other uncertainties in P_{soil} . At field sites with weathered regoliths, another source of uncertainty can arise in the correction factor that accounts for the bias in ^{10}Be concentrations due to quartz enrichment in the regolith (Small et al., 1999; Riebe et al., 2001a). At our field sites, the correction factor associated with this extended exposure is 1.68 ± 0.19 , and is the largest source of uncertainty in our P_{soil} estimates.

The uncertainties listed for all mineral abundances are a composite of two uncertainties. The first uncertainty is the standard error associated with the sample-to-sample variability in mineral abun-

dances, which was typically small (<1%). A more conservative means of estimating uncertainties in mineral abundances is to combine the sample-to-sample uncertainty with a methodological uncertainty associated with the XRD-based method itself. Our tests of FULLPAT on self-prepared mineral mixtures (Table 2) suggest that the uncertainties in XRD-based abundance determinations may depend on both mineral abundance and the mineral phase itself. Although our tests are not extensive enough to conclude how these methodological uncertainties depend on abundance for each mineral phase, they did reliably reproduce mineral abundances to 3.1% absolute or better over a range of abundances and a variety of mineral phases (Table 2), which is similar to accuracies reported by Chipera and Bish (2002). In particular, biotite appears to be resolvable at concentrations well below 1% absolute due to its strong peak at $10.19^\circ 2\theta$ (equivalent to a d-spacing of 10.07 \AA). To account for this methodological uncertainty, we conservatively added a 3% absolute uncertainty in quadrature to the sample-to-sample uncertainty in quartz, plagioclase, and hornblende, and a 0.4% absolute uncertainty to the uncertainty in biotite abundances. This resulted in mean bedrock mineral abundances that are still easily distinguishable from zero except for biotite at site RI-1. For the most abundant and most soluble minerals (here plagioclase and hornblende), the methodological uncertainty contributes a small fraction of the total uncertainty in estimated mineral weathering rates.

A final source of uncertainty, and one that we do not treat here, arises from the possible deviation of the regolith from steady state. Because the mass balance framework in Section 2 is founded on the assumption of a steady state regolith, the accuracy of mineral weathering rates estimated within this framework depends on the degree to which mass fluxes into the regolith differ from mass fluxes out of the regolith over the time of regolith development. We expect this effect to be small for our samples. The regolith samples analyzed here were collected from hillslope sites that had not experienced recent landsliding (Riebe et al., 2003), and modeling results suggest that errors in estimated chemical erosion rates should be smaller than fluctuations in physical erosion rates (Ferrier and Kirchner, 2008). That modeling study found, for example, that if physical erosion rates fluctuated by 50% of their long-term mean, estimates of chemical erosion rates calculated with the mass balance framework should deviate from actual chemical erosion rates by no more than 15%. Because several studies have suggested that the weathering system at Rio Iacacos is operating at close to steady state (Turner et al., 2003; Fletcher et al., 2006; Blaes et al., 2009), and because it is not the purpose of this paper to explore how deviations from steady state affect mineral weathering rates, we do not address this issue further here.

Table 3
Site RI-1 mineral abundances, weathering rates, and bulk fluxes (mean \pm s.e.).

	Mineral abundances (mol kg^{-1})			$W_{\text{regolith},X}$ ($\text{mol ha}^{-1} \text{yr}^{-1}$) ^b
	Bedrock	Soil	Dust ^a	
Quartz	3.76 ± 0.71	8.07 ± 0.68	2.30 ± 0.18	-373 ± 1368
Plagioclase	2.09 ± 0.13	0.04 ± 0.11	0.15 ± 0.01	3274 ± 575
Hornblende	0.13 ± 0.03	0.03 ± 0.04	0	187 ± 71
Biotite	0.009 ± 0.009	0.00 ± 0.01	0	14 ± 16
Zr (ppm) ^c	85 ± 9	205 ± 10	167 ± 12	
n	5 or 6 ^d	13		
Bulk rates		$\text{t km}^{-2} \text{yr}^{-1}$		Source
$P_{\text{soil}}^{\text{e}}$		113 ± 17		^{10}Be
$P_{\text{sap}}^{\text{f}}$		157 ± 18		Eq. (8)
P_d		21 ± 7		Pett-Ridge et al. (2009)
W_{regolith}		94 ± 17		Eq. (11)
E		84 ± 15		Eq. (3)

^a Dust mineral abundances taken from Glaccum and Prospero (1980) and dust Zr concentration from Herwitz et al. (1996).

^b $W_{\text{regolith},X}$ rates were calculated with Eq. (12) under the assumption that thick saprolite exists at RI-1 as it does elsewhere in the Rio Iacacos catchment, and that at RI-1 the ratio $Zr_{\text{sap}}/Zr_{\text{rock}}$ is 1.39 ± 0.07 , as was measured at the nearby RI-7 site (Riebe et al., 2003).

^c Zr concentrations in bedrock and soil from Riebe et al. (2003).

^d Because of a poor match between the measured XRD pattern of one rock sample (RI-1P4X) and standard mineral patterns for plagioclase and hornblende, we were not able to determine abundances for these minerals in that sample. The number of rock samples used for mean plagioclase and hornblende abundances is thus 5, while n for quartz and biotite is 6.

^e Soil production rate P_{soil} was calculated with version 2.2 of the CRONUS calculator (Balco et al., 2008) from Riebe et al.'s measurements of $1.83 \pm 0.14 \times 10^5$ atoms $^{10}\text{Be}/\text{g}$ quartz (Riebe et al., 2003), a topographic shielding factor of 0.937, and a quartz enrichment factor (Small et al., 1999; Riebe et al., 2001a) of 1.68 ± 0.19 .

^f Calculated with Eq. (8) assuming that $Zr_{\text{sap}}/Zr_{\text{rock}}$ is 1.39 ± 0.07 , as was measured at the nearby RI-7 site (Riebe et al., 2003).

5. Results and discussion

As Eqs. (1)–(14) demonstrate, estimated mineral weathering rates depend on measurements of soil production rates, dust deposition rates, immobile element concentrations, and mineral abundances. Because the ^{10}Be and Zr measurements are discussed in detail in Riebe et al. (2003) and the dust flux estimate is discussed in detail in Pett-Ridge et al. (2009), we focus here on the new mineral abundance data and new estimates of mineral weathering rates.

5.1. Mineral abundances

We measured mineral abundances in six rock samples and thirteen soil samples from site RI-1, and in five rock samples, thirteen saprolite samples, and 30 soil samples from site RI-4 based on the powder XRD patterns of each sample. Qualitatively, the mineralogic differences between rock and regolith can easily be seen by eye in the XRD patterns. Fig. 5 shows representative XRD patterns for one soil sample, one saprolite sample, and one rock sample from site RI-4, and

Table 4Site RI-4 mineral abundances, weathering rates, and bulk fluxes (mean \pm s.e.).

	Mineral abundances (mol kg^{-1})				Weathering rates ($\text{mol ha}^{-1} \text{yr}^{-1}$)		
	Bedrock	Saprolite	Soil	Dust ^a	$W_{\text{soil},X}^{\text{b}}$	$W_{\text{sap},X}^{\text{b}}$	$W_{\text{regolith},X}^{\text{b}}$
Quartz	3.62 ± 0.53	4.25 ± 0.51	9.47 ± 0.63	2.30 ± 0.18	-1468 ± 786	425 ± 962	-1043 ± 1002
Plagioclase	2.09 ± 0.14	0.04 ± 0.12	0.07 ± 0.11	0.15 ± 0.01	32 ± 170	3077 ± 541	3110 ± 530
Hornblende	0.22 ± 0.04	0.02 ± 0.04	0.03 ± 0.03	0	0 ± 53	308 ± 93	308 ± 85
Biotite	0.018 ± 0.010	0.00 ± 0.01	0.00 ± 0.01	0	0 ± 12	28 ± 18	28 ± 17
Zr (ppm) ^c	90 ± 2	115 ± 2	232 ± 8	167 ± 12			
n	3 or 5 ^d	13	30				
Bulk fluxes				$\text{t km}^{-2} \text{yr}^{-1}$			Source
$P_{\text{soil}}^{\text{e}}$				118 ± 17			^{10}Be
P_{sap}				151 ± 22			Eq. (8)
P_d				21 ± 7			Pett-Ridge et al. (2009)
W_{soil}				65 ± 10			Eq. (4)
W_{sap}				32 ± 12			Eq. (9)
W_{regolith}				98 ± 16			Eq. (11)
E				74 ± 11			Eq. (3)

^a Dust mineral abundances taken from Glaccum and Prospero (1980) and dust Zr concentration from Herwitz et al. (1996).^b $W_{\text{soil},X}$, $W_{\text{sap},X}$, and $W_{\text{regolith},X}$ are calculated with Eqs. (5), (10), and (12), respectively.^c Zr concentrations in bedrock, saprolite, and soil are from Riebe et al. (2003).^d Because of poor matches between the measured XRD patterns of two rock samples (RI-4X4 and RI-4X5) and standard mineral patterns for plagioclase, we were not able to determine abundances for plagioclase in those samples. The number of rock samples used for mean plagioclase abundances is thus 3, while n for quartz, hornblende, and biotite is 5.^e Soil production rate was calculated with version 2.2 of the CRONUS calculator (Balco et al., 2008) from Riebe et al.'s measurements of $1.76 \pm 0.10 \times 10^5$ atoms $^{10}\text{Be}/\text{g}$ quartz (Riebe et al., 2003), a topographic shielding factor of 0.902, and a quartz enrichment factor (Small et al., 1999; Riebe et al., 2001a) of 1.68 ± 0.19 .

the differences in the patterns reveal clear differences in mineralogy from sample to sample. The soil and saprolite patterns look quite similar – all of their sharp peaks come from quartz, kaolinite, and the corundum standard added to each sample – but they differ from the rock pattern in that they lack peaks between 32 and $40^\circ 2\theta$, reflecting the absence of plagioclase and hornblende. Clearly, these samples show that plagioclase and hornblende have been intensively weathered during the conversion of bedrock to saprolite, in agreement with measurements of elemental losses elsewhere in the Rio Iacacos basin (e.g., White et al., 1998; Turner et al., 2003; Buss et al., 2008).

FULLPAT analysis of these XRD patterns provides mineral abundance data that quantitatively confirm the large mineralogic differences between rock and regolith. As Tables 3 and 4 show, the

rock samples are dominated by quartz and feldspar, have less hornblende, and include trace amounts of biotite. What little biotite exists in the rock samples is completely absent in all of the saprolite and soil samples, and plagioclase and hornblende are both greatly depleted, if not completely depleted, in the saprolite and soil samples. Only one of the thirteen saprolite samples contains any measurable plagioclase or hornblende at all, while roughly two-thirds of the soil samples contain no measurable plagioclase, and about 40% of the soil samples contain no measurable hornblende. (See Table SF2 in the Supplementary file for mineral abundances in each of the 67 samples.) The saprolite samples do not show any mineralogic trends over the range of sampling depths (95 cm to 222 cm; Table SF2), which is consistent with observations that weathering at Rio Iacacos is concentrated in a narrow zone of saprock between bedrock and saprolite well below our deepest saprolite samples (e.g., White et al., 1998; Turner et al., 2003; Buss et al., 2008). Plagioclase and hornblende are more evenly distributed in the soil samples than in the saprolite samples, which is consistent with mixing of compositionally variable saprolite samples in the soil, and supports other observations of soil mixing at Rio Iacacos by earthworms, burrowing animals, and roots (e.g., White et al., 1998).

The FULLPAT-derived mineral abundances for quartz, plagioclase, and hornblende in rock, saprolite, and soil at RI-1 and RI-4 (Tables 3, 4) agree well with previous mineral abundance measurements made by point counting in samples of rock, saprolite, and soil collected in ridgetop weathering profiles elsewhere in the Rio Iacacos catchment (Murphy, 1995, as cited in White et al., 1998). The primary difference between mineral abundances at RI-1 and RI-4 and those measured elsewhere in the Rio Iacacos catchment is in biotite. This is true for both the rock samples and the regolith samples. In the rock samples at RI-1 and RI-4, abundances of biotite are much lower (9–18 mmol/kg) than in rock samples examined by Murphy (208 mmol/kg) (Murphy, 1995; White et al., 1998). Is this an indication that the FULLPAT-determined estimates of biotite abundances at sites RI-1 and RI-4 are too low by a factor of 10–20? Such a bias in calculated biotite abundances could arise if, during preparation of the standard biotite specimen, the biotite crystallites were oriented along a common crystal plane, which would artificially amplify the intensity of the dominant biotite peak relative to the corundum peaks against which the biotite peaks are normalized. Such preferred orientation can be especially strong in platy minerals like biotite, which within a powdered specimen may align themselves along basal planes rather than randomly (e.g.,

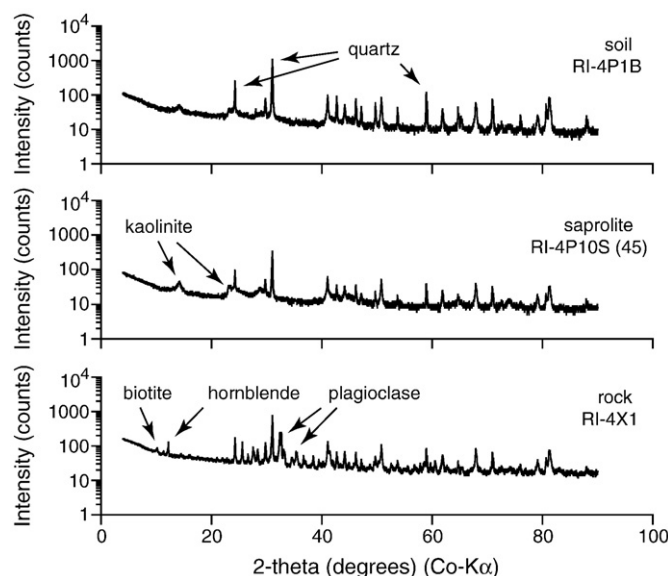


Fig. 5. Measured XRD patterns for one rock sample, one saprolite sample, and one soil sample from site RI-4. The absence of peaks between 32 and $40^\circ 2\theta$ in the saprolite and soil patterns show that the plagioclase present in the rock has been completely weathered, and the absence of peaks at 10.2 and $12.2^\circ 2\theta$ in the saprolite and soil samples similarly show that biotite and hornblende have also been completely weathered.

Jenkins and Snyder, 1996; Kleeberg et al., 2008). However, although preferred orientation can be important for biotite, our tests on self-prepared mineral mixtures suggest that preferred orientation has not dramatically skewed FULLPAT-calculated estimates of biotite concentrations (Fig. 4, Table 2). The FULLPAT-determined biotite abundance in this test ($5.2 \pm 0.2\%$) was only slightly lower than the true biotite abundance (5.6%) – far less than the order of magnitude difference in biotite concentrations between our samples at RI-1 and RI-4 and those in Murphy (1995). Thus we suggest preferred orientation is unlikely to have caused FULLPAT to calculate artificially low biotite abundances. Our measurements also suggest that FULLPAT-derived biotite abundances were not strongly affected by differences between the XRD pattern of the standard biotite and the biotite present in the Rio Icacos bedrock. To verify this, we measured the powder XRD pattern of biotite isolated from Rio Icacos bedrock (courtesy of Heather Buss, USGS, October 2007), and found that its XRD pattern did not differ substantially from the XRD pattern of the standard biotite used in FULLPAT. Thus our measurements suggest that FULLPAT-calculated biotite abundances were not severely skewed by preferred orientation or by a mismatch between the standard biotite and the biotite in sampled bedrock.

The biotite XRD patterns in saprolite and soil at RI-1 and RI-4 also differ from those in previous studies of soil and saprolite at Rio Icacos. In previous studies of biotite in a weathering profile elsewhere in the Rio Icacos catchment, the presence of an altered biotite phase with a lattice spacing of 10.5 \AA was inferred from powder XRD patterns (Murphy et al., 1998) and TEM measurements (Dong et al., 1998). In contrast to those studies, none of the XRD patterns of our soil and saprolite samples at RI-1 and RI-4 show a diffraction peak at 10.5 \AA (equivalent to $9.77^\circ 2\theta$ in Fig. 5). Because our measurements and those in Murphy et al. (1998) were both made with powder XRD, we suggest the difference between our XRD patterns and this in Murphy et al. (1998) is not a reflection of methodological differences. Instead, we suggest it is a reflection of geochemical differences between the samples studied in Murphy et al. (1998) and our samples at RI-1 and RI-4. Similarly, the absence of peaks at 10.07 \AA in the RI-1 and RI-4 saprolite and soil XRD patterns indicates that pristine biotite is not present in the RI-1 and RI-4 regolith samples. These XRD measurements suggest that biotite concentrations in rock and regolith samples at RI-1 and RI-4 are much lower than in rock and regolith samples collected elsewhere in the Rio Icacos catchment, and that the minor quantities of biotite in bedrock at RI-1 and RI-4 are completely weathered before reaching the upper saprolite.

5.2. Mineral-specific weathering rates

We combined the FULLPAT-derived mineral abundance measurements with prior measurements of Zr concentrations in the same samples (Riebe et al., 2003), new estimates of soil production rates (Section 4.1) from the ^{10}Be concentrations measured by Riebe et al. (2003), and a published dust deposition rate of $21 \pm 7 \text{ t km}^{-2} \text{ yr}^{-1}$ (Pett-Ridge et al., 2009). Because direct measurements of dust mineralogy and chemistry are unavailable at Rio Icacos, and because studies have found that variations in African dust composition are relatively small across the Caribbean (Glaccum and Prospero, 1980), we assume that the composition of African dust deposited at our field sites is the same as the composition of Saharan dust deposited at a long-term dust monitoring station in Barbados (Glaccum and Prospero, 1980; Herwitz et al., 1996) (Tables 3, 4). From these combined sets of measurements, we used Eqs. (5), (10), (12), and (14) to calculate chemical weathering rates for quartz, plagioclase, hornblende, and biotite (Tables 3 and 4 and Fig. 6).

As Fig. 6 shows, the bulk of the primary mineral weathering at Rio Icacos is due to plagioclase weathering, and nearly all of the remainder is accounted for by hornblende weathering. Because at RI-4 samples of saprolite, rock, and soil are available, we are able to estimate mineral weathering rates in both saprolite and soil, under the assumption that the composition and mass per unit area of both saprolite and soil remain

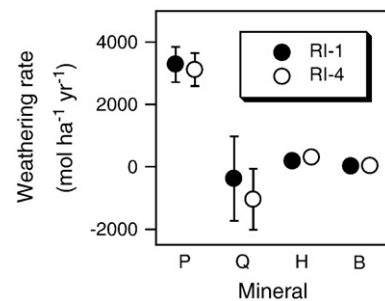


Fig. 6. Mineral-specific chemical weathering rates in the regolith at sites RI-1 and RI-4 for P: plagioclase, Q: quartz, H: hornblende, and B: biotite, as calculated with Eq. (12). Comparisons among these weathering rates illustrate the extent to which plagioclase weathering dominates total weathering at Rio Icacos.

steady over time. These data reveal major differences in weathering rates between the saprolite and the soil. Within uncertainty, all of the primary mineral weathering at RI-4 occurs between the bedrock and the upper saprolite at a depth of 222 cm (i.e., the depth of our deepest saprolite samples). This is consistent with the finding that the great majority of weathering at Rio Icacos occurs in the narrow zone of saprock between bedrock and saprolite (White et al., 1998; Turner et al., 2003; Buss et al., 2008). Plagioclase and hornblende are weathered nearly to completion below the upper saprolite, and biotite is completely lost; consequently, their weathering rates between the bedrock and the top of the saprolite (i.e., $W_{\text{saprolite},X}$) are high. Because the concentrations of these minerals at the top of the saprolite are so small, they are supplied to the soil in small quantities during soil production, and as a consequence their weathering rates in soil (i.e., $W_{\text{soil},X}$) are low.

These calculated weathering rates in the soil, saprolite, and regolith (Tables 3, 4) should be considered averages over the lengths of time the sampled material has been weathering in the soil, saprolite, and regolith. That is, these timescales are the transit times of the sampled material through the soil, saprolite, and regolith. Based on our measured soil production rates and the ranges in density and thickness of soil and saprolite at Rio Icacos, we estimate these timescales as 7–16 kyr in soil, 20–93 kyr in saprolite, and 27–109 kyr in regolith at our field sites. We calculate this timescale in soil as $\rho_{\text{soil}} H_{\text{soil}} / E$, where ρ_{soil} is the soil density ($1.19\text{--}1.37 \text{ g cm}^{-3}$; White et al., 1998), H_{soil} is the soil thickness (0.5–1 m; White et al., 1998), and E is the physical erosion rate estimated with Eq. (3). We similarly calculate this timescale in the saprolite as $\rho_{\text{sap}} H_{\text{sap}} / P_{\text{soil}}$, where ρ_{sap} is the saprolite density ($1.19\text{--}1.35 \text{ kg m}^{-3}$; White et al., 1998), H_{sap} is the saprolite thickness (2–8 m; White et al., 1998), and P_{soil} is the soil production rate inferred from cosmogenic ^{10}Be . This timescale in the regolith is the sum of the soil and saprolite residence times.

5.3. Comparison to prior measurements of mineral weathering rates

The framework we use to calculate mineral weathering rates at Rio Icacos yields rates in mineral mass per unit area of hillslope per time. These are the units of greatest interest in studies of landscape evolution and marine ecology that require measurements of catchment-scale mass fluxes. By contrast, many chemical weathering rates in the literature are reported as rates of mineral mass per unit area of mineral surface per time, which are the units of greatest interest in studies of grain-scale mineral dissolution mechanisms. Comparing rates estimated by different methods requires converting weathering rates from one set of units to the other, which requires calculating the ratio of mineral surface area to landscape surface area, which in turn requires measurements of mineral-specific surface area, regolith density, and mineral abundance throughout the weathering column from the surface down to bedrock. At Rio Icacos, these measurements are particularly important in the narrow zone of saprock between bedrock and saprolite where the majority of mineral weathering

occurs (White et al., 1998; Turner et al., 2003; Buss et al., 2008). We do not have these measurements at RI-1 and RI-4. Our soil samples at RI-1 are representative of the soil, not the saprolite, and at site RI-4 our deepest saprolite samples come from a depth of 222 cm (Table SF2, Supplementary file), well above the saprock. It would be inappropriate to extrapolate our mineral abundance data down to the bedrock–saprolite boundary. Instead, for the sake of comparison we convert previously published weathering rates to units of moles per unit area of hillslope per year, by methods described below. These rates are compiled in Table 5.

5.3.1. Plagioclase weathering rates

As calculated with Eqs. (5), (10), and (12), plagioclase weathering rates per unit area of hillslope are $3274 \pm 575 \text{ mol ha}^{-1} \text{ yr}^{-1}$ in the regolith at RI-1, $3077 \pm 541 \text{ mol ha}^{-1} \text{ yr}^{-1}$ in the saprolite at RI-4, and $32 \pm 170 \text{ mol ha}^{-1} \text{ yr}^{-1}$ within the soil at RI-4, confirming that the great majority of plagioclase weathering occurs below our deepest saprolite samples at 222 cm. (Turner et al., 2003) and (Buss et al., 2008) also measured in-situ plagioclase weathering rates in the Rio Iacisos catchment, and reported these rates in moles weathered per unit volume per time. To compare our measurements with theirs, we convert the reported rates of Turner et al. (2003) and Buss et al. (2008) to moles per unit area of hillslope per year as follows.

Turner et al.'s field sites (named GN and SS) were two zones of partially weathered rock that lay above unweathered corestones and below 1–2 m of regolith. As described in Turner et al. (2003), samples of weathered rock were collected from a cut stream bank at site GN and from a roadcut at site SS. Within these weathering zones, Turner et al. measured Na and Ti concentrations and, under the assumption that Ti is immobile, calculated volumetric weathering rates of 1.52×10^{-9} and $3.82 \times 10^{-9} \text{ mol Na m}^{-3} \text{ s}^{-1}$. Assuming that plagioclase is the sole source of Na in the parent rock and that each mole of plagioclase contains 0.6 moles of Na (Turner et al., 2003), these Na weathering rates translate to 2.53×10^{-9} and $6.37 \times 10^{-9} \text{ mol plagioclase m}^{-3} \text{ s}^{-1}$. These measurements were made over a zone 58 cm thick at site GN and 45 cm thick at

site SS. Multiplying the volumetric weathering rates by these thicknesses gives rates of 464 and 904 mol ha⁻¹ yr⁻¹ per year, respectively. These should be considered lower bounds on the total plagioclase weathering rates per unit area of hillslope at these sites, because some plagioclase still remains at the ends of the weathered rock sequences at GN and SS, and thus some plagioclase may be weathering simultaneously in the overlying regolith. At site GN, 46% of the original Na (and by extension, 46% of the original plagioclase) still exists at the end of the measured weathering zone, and at site SS 4% of the original Na remains at the end of the measured weathering zone. If all of the remaining plagioclase at each site weathered to completion in the overlying regolith, the total plagioclase weathering rates would be $464/(1 - 0.46) = 853 \text{ mol ha}^{-1} \text{ yr}^{-1}$ at GN and $904/(1 - 0.04) = 940 \text{ mol ha}^{-1} \text{ yr}^{-1}$ at SS. This suggests that plagioclase weathering rates per unit area of hillslope are at least 464 mol ha⁻¹ yr⁻¹ but no faster than 853 mol ha⁻¹ yr⁻¹ at GN, and at least 904 mol ha⁻¹ yr⁻¹ but no faster than 940 mol ha⁻¹ yr⁻¹ at SS. These ranges of possible weathering rates are over a factor of three slower than the plagioclase weathering rates calculated in this study at sites RI-1 and RI-4 and those measured by Buss et al. (2008), discussed below.

Buss et al. (2008), like Turner et al. (2003), measured the spatial gradient in solid-phase Na and Ti concentrations in a zone of weathered rock immediately above an unweathered corestone exposed in a roadcut. Assuming that Ti is immobile and Na is contained only within plagioclase, these measurements permit calculation of a volumetric plagioclase weathering rate. For comparison with the plagioclase weathering rates at RI-1 and RI-4, we converted Buss et al.'s volumetric plagioclase weathering rate to a plagioclase weathering rate per unit area of hillslope by multiplying the thickness of the zone over which Na and Ti concentrations were measured (53 cm) by the volumetric plagioclase weathering rate r_s ($516 \text{ mol m}^{-3} \text{ yr}^{-1}$). This value for the volumetric weathering rate was calculated as $r_s = \rho_{\text{rock}} \omega / (\beta b_s)$ (White, 2002), where ρ_{rock} (kg m^{-3}) is the density of the unweathered rock, ω (m yr^{-1}) is the advance rate of the weathering front, β (mol element/mol mineral) is the stoichiometric coefficient for the measured mobile element in the mineral of interest, and b_s (m kg mol^{-1}) is the reciprocal of the gradient in Ti-normalized Na concentrations. In using ρ_{rock} rather than the density of the weathered material we deviate from the expression in White (2002); we do this in order to resolve a minor dimensional inconsistency and to bring this expression into agreement with other established methods for calculating weathering rates (Stallard, 1985; Brimhall and Dietrich, 1987). From Buss et al.'s measurements of $\rho_{\text{rock}} = 2700 \text{ kg m}^{-3}$, $\omega = 4.3 \times 10^{-5} \text{ m/yr}$, $\beta = 0.5 \text{ mol Na/mol plagioclase}$, and $b_s = 0.45 \text{ m kg mol}^{-1}$, we calculate a plagioclase weathering rate of $2735 \text{ mol ha}^{-1} \text{ yr}^{-1}$. Four percent of the parent Na remains at the top of this 53 cm weathering zone, implying that the total plagioclase weathering rate per unit area of hillslope at this site is likely to be no faster than $2735/(1 - 0.04) = 2849 \text{ mol ha}^{-1} \text{ yr}^{-1}$. This range of possible plagioclase weathering rates agrees with our calculated plagioclase weathering rates at RI-1 and RI-4 within uncertainty.

5.3.2. Hornblende weathering rates

As calculated with Eqs. (5), (10), and (12), hornblende weathering rates per unit area of hillslope are $187 \pm 71 \text{ mol ha}^{-1} \text{ yr}^{-1}$ in the regolith at RI-1, $308 \pm 93 \text{ mol ha}^{-1} \text{ yr}^{-1}$ in the saprolite at RI-4, and $0 \pm 53 \text{ mol ha}^{-1} \text{ yr}^{-1}$ in the soil at RI-4 (Table 5). These are 1.5–2.5 times slower than hornblende weathering rates reported in Buss et al. (2008), who inferred these rates from measurements of the gradient in Ti-normalized Fe(II) concentrations across a 7 cm zone of protosaprolite exposed in a roadcut. We have normalized Buss et al.'s volumetric hornblende weathering rate to a weathering rate per unit area of hillslope by multiplying the thickness of the protosaprolite (7 cm) by the volumetric weathering rate r_s within the protosaprolite ($677 \text{ mmol m}^{-3} \text{ yr}^{-1}$, calculated as $r_s = \rho_{\text{rock}} \omega / (\beta b_s)$ using Buss et al.'s measurements of $\rho_{\text{rock}} = 2700 \text{ kg m}^{-3}$, $\omega = 4.3 \times 10^{-5} \text{ m/yr}$, $\beta = 0.063 \text{ mol Fe(II)/mol hornblende}$, and $b_s = 0.088 \text{ m kg mol}^{-1}$). The resulting hornblende

Table 5
Rio Iacisos mineral weathering rates.

Weathering rate			
	(mol ha ⁻¹ yr ⁻¹) ^a	Method	Source
Quartz	-373 ± 1368	Eq. (12)	RI-1 regolith, this study
	425 ± 962	Eq. (10)	RI-4 saprolite, this study
	-1468 ± 786	Eq. (5)	RI-4 soil, this study
	228^b	Porewater chemistry	Schulz and White (1999)
Plagioclase	3274 ± 575	Eq. (12)	RI-1 regolith, this study
	3077 ± 541	Eq. (10)	RI-4 saprolite, this study
	32 ± 170	Eq. (5)	RI-4 soil, this study
	$\geq 464^c$	Solid-phase Na, Ti	Turner et al. (2003), site GN
	$\geq 904^c$	Solid-phase Na, Ti	Turner et al. (2003), site SS
	2735^c	Solid-phase Na, Ti	Buss et al. (2008)
Hornblende	187 ± 71	Eq. (12)	RI-1 regolith, this study
	308 ± 93	Eq. (10)	RI-4 saprolite, this study
	0 ± 53	Eq. (5)	RI-4 soil, this study
	474^c	Solid-phase Fe(II), Ti	Buss et al. (2008)
Biotite	14 ± 16	Eq. (12)	RI-1 regolith, this study
	28 ± 18	Eq. (10)	RI-4 saprolite, this study
	0 ± 12	Eq. (5)	RI-4 soil, this study
	500 ± 920	Porewater K, Mg	Murphy et al. (1998)
	461 ± 990^c	Porewater K, Mg	White (2002)
	734^c	Solid-phase Fe(II), Ti	Buss et al. (2008)

^a Means and standard errors are denoted with a \pm symbol, e.g. 187 ± 71 , and ranges are indicated with a dash, e.g. 500 ± 920 .

^b Quartz weathering rates from Schulz and White (1999) were calculated by multiplying the reported mean quartz weathering rate ($1.6 \times 10^{-15} \text{ mol m}^{-2} \text{ of mineral s}^{-1}$) by the reported total quartz surface area in a 1 m^2 column of saprolite ($4.55 \times 10^5 \text{ m}^2 \text{ of mineral per m}^2 \text{ of saprolite}$).

^c Calculated by multiplying the volumetric weathering rate by the thickness of the zone over which the rate measurement was made. See text for details.

weathering rate per unit area of hillslope is $474 \text{ mol ha}^{-1} \text{ yr}^{-1}$. Because, as Buss et al. noted, hornblende is completely weathered across this 7 cm zone, this represents a maximum possible hornblende weathering rate per unit area of hillslope at this site.

5.3.3. Biotite weathering rates

As calculated with Eqs. (10) and (12), biotite weathering rates per unit area of hillslope are $14 \pm 16 \text{ mol ha}^{-1} \text{ yr}^{-1}$ in the regolith at RI-1 and $28 \pm 18 \text{ mol ha}^{-1} \text{ yr}^{-1}$ in the saprolite at RI-4. These are much slower than previously reported biotite weathering rates at Rio Iacacos (Murphy et al., 1998; White, 2002; Buss et al., 2008), primarily because bedrock biotite abundances are much lower at RI-1 and RI-4 than in the rock samples examined in other studies, as discussed in Section 5.1. Murphy et al. (1998) reported biotite weathering rates in saprolite at Rio Iacacos of 500 and $920 \text{ mol ha}^{-1} \text{ yr}^{-1}$ based on vertical gradients in porewater concentrations of K and Mg, respectively. In White (2002), measurements of vertical gradients in porewater K and Mg concentrations over a 7.3 m saprolite profile permit calculation of volumetric biotite weathering rates of $6\text{--}14 \text{ mmol m}^{-3} \text{ yr}^{-1}$. Both Murphy et al. (1998) and White (2002) conducted their measurements in saprolite on a stable ridgeline. In contrast to the solute-based measurements of Murphy et al. (1998) and White (2002), Buss et al. (2008) measured Ti-normalized Fe(II) concentrations across a 46-cm zone of weathered rock in a corestone exposed in a roadcut, which permit calculation of a volumetric biotite oxidation rate of $160 \text{ mmol m}^{-3} \text{ yr}^{-1}$ (calculated as $r_s = \rho_{\text{rock}}\omega / (\beta b_s)$) and $\rho_{\text{rock}} = 2700 \text{ kg m}^{-3}$, $\omega = 4.3 \times 10^{-5} \text{ myr}$, $\beta = 0.36 \text{ mol Fe(II)/mol biotite}$, and $b_s = 2.02 \text{ m kg mol}^{-1}$). Multiplying the volumetric weathering rates in White (2002) and Buss et al. (2008) by the thicknesses of the zones over which each rate was measured yields biotite weathering rates of $461\text{--}990 \text{ mol ha}^{-1} \text{ yr}^{-1}$ and $734 \text{ mol ha}^{-1} \text{ yr}^{-1}$, respectively.

At this point it is useful to note that different methodologies for measuring biotite weathering rates may reflect different portions of the overall transformation of biotite to kaolinite. In our XRD-based approach, for example, biotite weathering is recognized by (and indeed can only be recognized by) changes to XRD patterns between unweathered and weathered samples. Thus the expansion of biotite to form vermiculite, which is the first step in the overall transformation of biotite to kaolinite, is classified as biotite weathering in our XRD-based approach because it alters biotite's crystal structure and thus its XRD pattern. In this respect the functional definition of biotite weathering in our study differs from that in Murphy et al. (1998) and White (2002), which recognized biotite weathering by the release of K and Mg to solution, which itself occurs during the initial transformation of biotite to vermiculite as well as during the further transformation of vermiculite to kaolinite. By contrast, our XRD-based definition of biotite weathering refers to a process similar to the biotite oxidation documented by Buss et al. (2008), because both crystal expansion and oxidation of Fe(II) to Fe(III) occur during the initial weathering of biotite to vermiculite.

5.3.4. Quartz weathering rates

As calculated with Eqs. (10) and (12), quartz weathering rates in the regolith at RI-1 and in the saprolite at RI-4 overlap zero within uncertainty ($-373 \pm 1368 \text{ mol ha}^{-1} \text{ yr}^{-1}$ and $425 \pm 962 \text{ mol ha}^{-1} \text{ yr}^{-1}$, respectively), as expected for a mineral so resistant to dissolution. These rates are also indistinguishable from the quartz weathering rate reported in Schulz and White (1999), which was calculated based on porewater chemistry in a ridgeline saprolite profile (Table 5). Within the soil at RI-4, however, Eq. (5) yield a quartz weathering rate that is negative beyond one standard error ($-1468 \pm 786 \text{ mol ha}^{-1} \text{ yr}^{-1}$), implying an apparent gain of quartz relative to Zr in the soil. Below we discuss several ways in which this calculated negative quartz weathering rate could arise.

One possibility, however unlikely, is that the calculated negative quartz weathering rate in RI-4 soil reflects mobility of Zr relative to quartz in the soil. Although zircon has a very low solubility and is thus

unlikely to lose much mass by chemical weathering, it is not perfectly insoluble: some studies have documented chemical mobility of Zr in the lab (Hodson, 2002) and in the field (Hill et al., 2000; Kurtz et al., 2000). Quartz, like zircon, has a very low solubility. In fact, its solubility is so low that some studies have used it as an immobile tracer in soils (e.g., White et al., 1996). Thus we expect chemical losses of quartz in Rio Iacacos soils to be small. However, although zircon may not be perfectly insoluble and quartz is highly resistant to dissolution, it is difficult to argue that chemical losses of quartz should be smaller than those of Zr. We expect the solubility of zircon to be at least as low as the solubility of quartz, and given prior documentation of quartz dissolution in Rio Iacacos saprolite (Schulz and White, 1999), we consider it unlikely that chemical losses of quartz in Rio Iacacos soils are less than those of Zr.

The calculated negative quartz weathering rate in RI-4 soil could also arise if Zr were more physically mobile than quartz in the soil. This could happen if zircons were physically segregated from quartz due to differences in grain size or density, as has been observed in bioturbated soils elsewhere (e.g., Colin et al., 1993). If the strong bioturbation in Rio Iacacos soils were to physically segregate zircons from quartz, it is theoretically possible that zircons could be concentrated in areas within the soil profile where physical erosion is fastest, which would lead to faster physical erosion of Zr than quartz. In other words, intense soil mixing might make Zr more physically mobile than quartz, which could account for the measured enrichment of quartz relative to Zr in RI-4 soils. Testing this would require in-situ measurements of downslope soil velocities at a number of depths within the soil column and co-located measurements of Zr and quartz concentrations. Our limited soil samples cannot test this, but we acknowledge that preferential physical mobility of Zr is a possibility at Rio Iacacos, as it is at any field site, and we note that this possibility is consistent with the observation of a quartz-rich layer at 40 cm depth in Rio Iacacos soils (Schulz and White, 1999).

Differences in chemical or physical mobility between quartz and Zr are not the only possible explanations for the calculated negative quartz weathering rate. If the dust deposition rate were a factor of five smaller than that determined by Pett-Ridge et al. (2009) (e.g., $4 \pm 4 \text{ t km}^{-2} \text{ yr}^{-1}$ instead of $21 \pm 7 \text{ t km}^{-2} \text{ yr}^{-1}$) or if the average dust Zr concentration were over a factor of two smaller than that determined by Herwitz et al. (1996) (e.g., $77 \pm 12 \text{ ppm}$ instead of $167 \pm 12 \text{ ppm}$), then the chemical weathering rate of quartz in RI-4 soils would be indistinguishable from zero, as expected. However, we suggest such a low dust deposition rate is unlikely because it is incompatible with Pett-Ridge et al.'s measurements of Sr fluxes and isotopic signatures in the Rio Iacacos catchment, and inconsistent with Herwitz et al.'s reported Zr concentrations.

Overall, we cannot definitively rule out any of these possible explanations for the calculated negative quartz weathering rate in RI-4 soil. We suggest, however, that it is unlikely that Zr is more chemically mobile than quartz or that dust deposition rates are at least five times lower than that reported in Pett-Ridge et al. (2009). We therefore suggest that it is more likely that Zr and quartz have similarly low chemical mobilities in Rio Iacacos soils and that the negative calculated quartz weathering rate may be indicative of enhanced physical mobility of Zr. As such, this dataset reinforces the importance of measuring mineral abundances as well as elemental abundances in chemical weathering studies. Because both quartz and Zr should both be approximately chemically immobile, the rock-to-soil enrichment of highly abundant and deeply insoluble minerals like quartz can serve as a check on the rock-to-soil enrichments of trace elements like Zr, whose low concentrations may be more easily skewed by secondary mass influxes into the soil or physical segregation.

5.3.5. Kaolinite weathering rates

In addition to weathering rates of primary minerals, this method can yield production rates of secondary minerals, provided that their

abundances can be accurately quantified. At Rio Icacos, kaolinite is the most abundant secondary mineral, and it manifests itself in the soil and saprolite XRD patterns as several sharp peaks (most prominently at $14.2^\circ 2\theta$) and two broad bulges at $23\text{--}31^\circ$ and $40\text{--}46^\circ 2\theta$. Our attempts to isolate from our soil samples a pure kaolinite standard with diffraction characteristics matching those in the regolith XRD patterns were unsuccessful, and as a consequence we were unable to use measured XRD patterns to reliably estimate the absolute abundances of kaolinite in our soil and saprolite samples. However, the intensities of the kaolinite peaks in the soil XRD patterns relative to those in the saprolite XRD patterns implies that kaolinite abundances in the soil are $36 \pm 6\%$ of kaolinite abundances in the saprolite, which is similar to the findings of Murphy (1995) (as cited in White et al., 1998), who reported a $[\text{kaolinite}]_{\text{soil}}/[\text{kaolinite}]_{\text{saprolite}}$ ratio of 46%. If we assume that the measured kaolinite abundances of Murphy (1995) – i.e. $[\text{kaolinite}]_{\text{rock}} = 0\%$, $[\text{kaolinite}]_{\text{saprolite}} = 59.4\%$, and $[\text{kaolinite}]_{\text{soil}} = 27.1\%$ – are representative of site RI-4, then Eqs. (5), (10), and (12) yield weathering rates for kaolinite of $W_{\text{soil,kaolinite}} = 2006 \pm 345 \text{ mol ha}^{-1} \text{ yr}^{-1}$, $W_{\text{sap,kaolinite}} = -2711 \pm 413 \text{ mol ha}^{-1} \text{ yr}^{-1}$ (where the negative sign denotes net production, rather than weathering, of kaolinite), and $W_{\text{regolith,kaolinite}} = -704 \pm 131 \text{ mol ha}^{-1} \text{ yr}^{-1}$. This suggests that the rate of kaolinite weathering in the soil is nearly three-quarters the rate of kaolinite production in the saprolite. These inferred losses of kaolinite in the soil are consistent with documented losses of aluminum between the saprolite and the soil at site RI-4 (Riebe et al., 2003) and are also consistent with the conclusions of (White et al., 1998), who measured an increase in the median grain size of kaolinite in soil relative to saprolite, which they suggest indicates preferential dissolution of the fine-grained kaolinite particles in the soil.

These estimates of kaolinite production rates in saprolite and kaolinite weathering rates in soil rely on the assumption that kaolinite does not migrate through the regolith once produced. If kaolinite were instead produced in the soil and translocated downwards into saprolite, then our estimates of kaolinite production rates in saprolite and kaolinite weathering rates in soil would be too high. For kaolinite translocation to greatly affect kaolinite abundances in the soil and saprolite, however, kaolinite production from weathering of plagioclase and biotite would need to be significant in the soil. We can be reasonably certain that this is not the case at Rio Icacos because virtually all of the plagioclase and biotite is weathered when bedrock is converted to saprolite, well below the soil–saprolite boundary. Thus we expect that translocation of kaolinite from the soil to the saprolite should have a negligible effect on kaolinite abundances in soil and saprolite, and thus a negligible effect on estimated rates of kaolinite weathering and production.

5.4. How much does dust deposition affect estimates of chemical and physical erosion rates?

At the time of Riebe et al.'s measurements of Zr and ^{10}Be (Riebe et al., 2003), no independent estimates of dust deposition rates were available at Rio Icacos, and Riebe et al. calculated bulk chemical and physical erosion rates under the assumption of negligible dust deposition. The new Rio Icacos dust flux estimate of Pett-Ridge et al. (2009) now permits incorporation of dust fluxes into the steady state mass balance model, and it demands a reevaluation of bulk chemical and physical erosion rates at sites RI-1 and RI-4. These updated estimates for bulk chemical and physical erosion rates are listed in Tables 3 and 4.

The updated estimates show that although a dust deposition rate of $21 \pm 7 \text{ t km}^{-2} \text{ yr}^{-1}$ is non-negligible relative to the inferred soil production rates of $113 \pm 17 \text{ t km}^{-2} \text{ yr}^{-1}$ and $118 \pm 17 \text{ t km}^{-2} \text{ yr}^{-1}$, it has only a small effect on estimates of bulk chemical erosion rates at our field sites. Ignoring dust fluxes in Eq. (11) (i.e., assuming $P_d \rightarrow 0$) yields mean estimates of 91 and $92 \text{ t km}^{-2} \text{ yr}^{-1}$ for W_{regolith} at RI-1 and RI-4, respectively, and including dust fluxes in Eq. (11) increases those

mean estimates to 94 and $98 \text{ t km}^{-2} \text{ yr}^{-1}$ at RI-1 and RI-4, respectively. Including dust fluxes in this mass balance model has a larger effect on estimates of physical erosion rates, which are 26% larger at each site than they would be if dust fluxes were assumed negligible in Eq. (3). Thus our updated calculations show that dust fluxes play a secondary but non-trivial role in setting bulk chemical and physical erosion rates at Rio Icacos, in agreement with the conclusions of Pett-Ridge et al. (2009).

6. Conclusions

The central purpose of this paper is to show that quantitative analysis of powder XRD patterns can – at least in samples with relatively simple mineralogies – yield mineral abundances that are accurate enough to be profitably used in the solid-phase mass balance approach for estimating long-term mineral weathering rates, even in places where dust deposition rates are high. In addition to measurements of mineral abundances, this mass balance approach requires measurements of soil production rates, dust deposition rates, and immobile element concentrations in the soil, saprolite, parent rock, and dust. The mathematical framework in which these measurements are used to calculate weathering rates is not new. Rather, the framework is an extension of the approach put forth by Stallard (1985), and it follows previous studies in its consideration of hillslopes where dust fluxes are significant and where saprolite weathering constitutes a major fraction of the total weathering (Owen et al., 2008; Dixon et al., 2009).

To demonstrate that uncertainties in calculated mineral weathering rates are not so large that they negate the utility of this solid-phase mass balance approach, we applied this approach to two sites in the Rio Icacos catchment of Puerto Rico. Our new XRD-based mineral abundances, when combined with prior measurements of soil production rates, immobile element concentrations, and estimates of dust deposition rate and dust composition, suggest that field-based weathering rates of abundant, soluble mineral phases can be accurately determined on eroding hillslopes in both saprolite and soil. At these field sites chemical weathering has stripped the saprolite and the soil of nearly all of its plagioclase and hornblende, and for these minerals, these measurements yield mineral weathering rates with uncertainties that are 17% of the mean for plagioclase and 37% or less of the mean for hornblende. These rates are averaged over the transit time of material through the saprolite and soil, which at these field sites have ranges of 20–93 kyr and 10–23 kyr, respectively.

Our measurements at Rio Icacos suggest the utility of this approach for estimating mineral weathering rates is primarily limited by uncertainties in cosmogenic-based soil production rates and XRD-based mineral abundances. Although many studies have measured soil production rates with cosmogenic nuclides (e.g., Heimsath et al., 1997; Riebe et al., 2001a; Dixon et al., 2009) and quantified mineral abundances with powder XRD (e.g., Hillier, 2000; Chipera and Bish, 2002; Omotoso et al., 2006; Andrews and Eberl, 2007; Jeong et al., 2008; Eberl and Smith, 2009), we do not mean to suggest that these measurements are trivial or universally applicable. Inferring soil production rates from cosmogenic nuclides requires assuming that the hillslope soil is in steady state (which is not true everywhere) and requires accurately assessing quartz enrichment in the soil (which can be difficult without direct measurements of quartz abundances). Quantifying mineral abundances with powder XRD patterns can be hampered by factors that confound interpretation of measured XRD patterns (e.g., preferred orientation, crystallite size, and variations in the crystallinity of a given mineral phase (Jenkins and Snyder, 1996; Kleeberg et al., 2008)). Thus powder XRD patterns are most likely to yield accurate abundances for high-abundance minerals with consistent crystallinities (e.g., quartz in granite), and are least likely to be useful for minerals that have crystal structures that vary between samples (e.g., poorly ordered clays) or that are present in trace quantities (e.g., calcite in granite). With these caveats, however, our measurements at Rio Icacos suggest that – at least at sites that are

close to erosional steady state and which have relatively simple mineralogies, like Rio Icacos – cosmogenic-based soil production rates and XRD-based mineral abundances can be accurate enough to yield useful estimates of long-term mineral weathering rates. Because this mass balance approach for estimating mineral weathering rates also depends on distinguishing the composition of the regolith from the composition of the parent material, the weathering rates it yields are most accurate in field settings where weathering has been intense and the regolith mineralogy is easily distinguishable from the parent mineralogy. Thus this approach is best suited to sites where chemical weathering is fast enough to produce a soil mineralogy that is easily distinguishable from the parent mineralogy, such as Rio Icacos, the southern Appalachians (e.g., White, 2002) or the mountains of Sri Lanka (e.g., von Blanckenburg et al., 2004). We suggest that the suite of measurements used in this paper may also be fruitfully applied at other eroding hillslopes, and that this approach can be useful in building a database of long-term mineral weathering rates that can help clarify how factors such as temperature, precipitation, vegetation, and physical erosion rates influence mineral weathering.

Appendix A. Supplementary data

Supplementary materials related to this article can be found online at doi:10.1016/j.chemgeo.2010.07.013.

References

- Alexander, L.E., Klug, H.P., Kummer, E., 1948. Statistical factors affecting the intensity of X-rays diffracted by crystalline powders. *Journal of Applied Physics* 19, 742–753.
- Anbeek, C., van Breemen, N., Meijer, E.L., van der Plas, L., 1994. The dissolution of naturally weathered feldspar and quartz. *Geochimica et Cosmochimica Acta* 58, 4601–4613.
- Andrews, J.T., Eberl, D.D., 2007. Quantitative mineralogy of surface sediments on the Iceland shelf, and application to down-core studies of Holocene ice rafted sediments. *Journal of Sedimentary Research* 77, 469–479.
- Balco, G., Stone, J.O., Lifton, N.A., Dunai, T.J., 2008. A complete and easily accessible means of calculating surface exposure ages or erosion rates from ^{10}Be and ^{26}Al measurements. *Quaternary Geochronology* 3, 174–195.
- Berner, R.A., Lasaga, A.C., Garrels, R.M., 1983. The carbonate–silicate geochemical cycle and its effect on atmospheric carbon dioxide over the past 100 million years. *American Journal of Science* 283, 641–683.
- Blaes, E., Chabaux, F., Pelt, E., Dosseto, A., Buss, H., White, A., Brantley, S., 2009. U-series constraints for the rate of bedrock–saprolite transformation in the Rio Icacos watershed, Puerto Rico. *Geochimica et Cosmochimica Acta* 73, A128.
- Brimhall, G.H., Dietrich, W.E., 1987. Constitutive mass balance relations between chemical composition, volume, density, porosity, and strain in metasomatic hydrochemical systems: results on weathering and pedogenesis. *Geochimica et Cosmochimica Acta* 51, 567–587.
- Brown, E.T., Stallard, R.F., Larsen, M.C., Raisbeck, G.M., You, F., 1995. Denudation rates determined from the accumulation of in situ-produced ^{10}Be in the Luquillo Experimental Forest, Puerto Rico. *Earth and Planetary Science Letters* 129, 193–202.
- Buss, H.L., Bruns, M.A., Schultz, M.J., Moore, J., Mathur, C.F., Brantley, S.L., 2005. The coupling of biological iron cycling and mineral weathering during saprolite formation, Luquillo Mountains, Puerto Rico. *Geobiology* 3, 247–260.
- Buss, H.L., Sak, P.B., Webb, S.M., Brantley, S.L., 2008. Weathering of the Rio Blanco quartz diorite, Luquillo Mountains, Puerto Rico: coupling oxidation, dissolution, and fracturing. *Geochimica et Cosmochimica Acta* 72, 4488–4507.
- Chipera, S.J., Bish, D.L., 2002. FULLPAT: a full-pattern quantitative analysis program for X-ray powder diffraction using measured and calculated patterns. *Journal of Applied Crystallography* 35, 744–749.
- Chou, L., Wollast, R., 1984. Study of the weathering of albite at room temperature and pressure with a fluidized bed reactor. *Geochimica et Cosmochimica Acta* 48, 2205–2217.
- Chung, F.H., 1974. Quantitative interpretation of X-ray diffraction patterns of mixtures. 1. Matrix-flushing method for quantitative multicomponent analysis. *Journal of Applied Crystallography* 7, 519–525.
- Clayton, J.L., 1986. An estimate of plagioclase weathering rate in the Idaho Batholith based upon geochemical transport rates. In: Colman, S.M., Dethier, D.P. (Eds.), *Rates of Chemical Weathering of Rocks and Minerals*. Academic Press, pp. 453–466, chapter 19.
- Cleaves, E.T., Godfrey, A.E., Bricker, O.P., 1970. Geochemical balance of a small watershed and its geomorphic implications. *Geological Society of America Bulletin* 81, 3015–3032.
- Clow, D.W., Drever, J.I., 1996. Weathering rates as a function of flow through an alpine soil. *Chemical Geology* 132, 131–141.
- Colin, F., Alarcon, C., Vielard, P., 1993. Zircon: an immobile index in soils? *Chemical Geology* 107, 273–276.
- Dixon, J.L., Heimsath, A.M., Amundson, R., 2009. The critical role of climate and saprolite weathering in landscape evolution. *Earth Surface Processes and Landforms* 1507–1521.
- Dong, H., Peacor, D.R., Murphy, S.F., 1998. TEM study of progressive alteration of igneous biotite to kaolinite throughout a weathered soil profile. *Geochimica et Cosmochimica Acta* 62, 1881–1887.
- Eberl, D.D., Smith, D.B., 2009. Mineralogy of soils from two continental-scale transects across the United States and Canada and its relation to soil geochemistry and climate. *Applied Geochemistry* 24, 1394–1404.
- Ferrier, K.L., Kirchner, J.W., 2008. Effects of physical erosion on chemical denudation rates: a numerical modeling study of soil-mantled hillslopes. *Earth and Planetary Science Letter* 272, 591–599.
- Ferrier, K.L., Kirchner, J.W., Finkel, R.C., 2005. Erosion rates over millennial and decadal timescales at Caspar Creek and Redwood Creek, Northern California Coast Ranges. *Earth Surface Processes and Landforms* 30, 1025–1038.
- Fletcher, R.C., Buss, H.L., Brantley, S.L., 2006. A spheroidal weathering model coupling porewater chemistry to soil thicknesses during steady-state denudation. *Earth and Planetary Science Letters* 244, 444–457.
- Garrels, R.M., Mackenzie, F., 1967. Origin of the chemical compositions of some springs and lakes. In: Colman, S.M., Dethier, D.P. (Eds.), *Advances in Chemistry Series*, 67. American Chemical Society, pp. 222–242.
- Glaccum, R.A., Prospero, J.M., 1980. Saharan aerosols over the tropical North Atlantic – mineralogy. *Marine Geology* 37, 295–321.
- Gosse, J.C., Phillips, F.M., 2001. Terrestrial in situ cosmogenic nuclides: theory and application. *Quaternary Science Reviews* 20, 1475–1560.
- Granger, D.E., Kirchner, J.W., Finkel, R., 1996. Spatially averaged long-term erosion rates measured from in situ-produced cosmogenic nuclides in alluvial sediment. *Journal of Geology* 104, 249–257.
- Green, E.G., Dietrich, W.E., Banfield, J.F., 2006. Quantification of chemical weathering rates across an actively eroding hillslope. *Earth and Planetary Science Letters* 242, 155–169.
- Heimsath, A.M., Dietrich, W.E., Nishizumi, K., Finkel, R.C., 1997. The soil production function and landscape equilibrium. *Nature* 388, 358–361.
- Herwitz, S.R., Muhs, D.R., Prospero, J.M., Mahan, S., Vaughn, B., 1996. Origin of Bermuda's clay-rich Quaternary paleosols and their paleoclimatic significance. *Journal of Geophysical Research* 101, 23389–23400.
- Hill, I.G., Worden, R.H., Meighan, I.G., 2000. Yttrium: the immobility–mobility transition during basalt weathering. *Geology* 28, 923–926.
- Hillier, S., 2000. Accurate quantitative analysis of clay and other minerals in sandstones by XRD: comparison of a Rietveld and a reference intensity ratio (RIR) method and the importance of sample preparation. *Clay Minerals* 35, 291–302.
- Hodson, M.E., 2002. Experimental evidence for mobility of Zr and other trace elements in soils. *Geochimica et Cosmochimica Acta* 66, 819–828.
- ICDD, 2003. Powder Diffraction File 2, Release 2003. International Center for Diffraction Data, 12 Campus Boulevard, Newton Square, Pennsylvania, USA, 19073.
- Jenkins, R., Snyder, R.L., 1996. *Introduction to X-ray Powder Diffractometry*. John Wiley and Sons.
- Jeong, G.I., Hillier, S., Kemp, R.A., 2008. Quantitative bulk and single-particle mineralogy of a thick Chinese loess–paleosol section: implications for loess provenance and weathering. *Quaternary Science Reviews* 27, 1271–1287.
- Kleeborg, R., Monecke, T., Hillier, S., 2008. Preferred orientation of mineral grains in sample mounts for quantitative XRD measurements: how random are powder samples? *Clays and Clay Minerals* 56, 404–415.
- Kurtz, A.C., Derry, L.A., Chadwick, O.A., Alfano, M.J., 2000. Refractory element mobility in volcanic soils. *Geology* 28, 683–686.
- Lal, D., 1991. Cosmic ray labeling of erosion surfaces: in situ nuclide production rates and erosion models. *Earth and Planetary Science Letters* 104, 424–439.
- Larsen, M.C., 1997. Tropical geomorphology and geomorphic work: a study of geomorphic processes and sediment and water budgets in montane humid-tropical forested and developed watersheds, Puerto Rico. Ph.D. thesis, University of Colorado.
- Larsen, M.C., Simon, A., 1993. A rainfall intensity-duration threshold for landslides in humid-tropical environment, Puerto Rico. *Geographiska Annaler Series A – Physical Geography* 75.
- Larsen, M.C., Torres-Sanchez, A.J., Concepcion, I.M., 1999. Slopewash, surface runoff and fine-litter transport in forest and landslide scars in humid-tropical steeplands, Luquillo Experimental Forest, Puerto Rico. *Earth Surface Processes and Landforms* 24, 481–502.
- Mahowald, N.M., Muhs, D.R., Levis, S., Rasch, P.J., Yoshioka, M., Bender, C.S., Luo, C., 2006. Change in atmospheric mineral aerosols in response to climate: last glacial period, preindustrial, modern, and doubled carbon dioxide climates. *Journal of Geophysical Research* 111, D10202.
- McDowell, W.H., Asbury, C.E., 1994. Export of carbon, nitrogen, and major ions from three tropical montane watersheds. *Limnology and Oceanography* 39, 111–125.
- Merritts, D.J., Chadwick, O.A., Hendricks, D.M., 1991. Rates and processes of soil evolution on upland marine terraces, northern California. *Geoderma* 51, 241–275.
- Mudd, S.M., Furbish, D.J., 2004. Influence of chemical denudation on hillslope morphology. *Journal of Geophysical Research* 109, F02001.
- Muhs, D.R., Bush, C.A., Stewart, K.D., Rowland, T.R., Crittenden, R.C., 1990. Geochemical evidence of Saharan dust parent material for soils developed on Quaternary limestones of Caribbean and western Atlantic islands. *Quaternary Research* 33, 157–177.
- Muhs, D.R., Budahn, J.R., Prospero, J.M., Carey, S.N., 2007. Geochemical evidence for African dust inputs to soils of western Atlantic islands: Barbados, the Bahamas, and Florida. *Journal of Geophysical Research* 112, F02009.

- Murphy, S.F., 1995. The weathering of biotite in a tropical forest soil, Luquillo Mountains, Puerto Rico. Master's thesis, Penn State University.
- Murphy, S.F., Brantley, S.L., Blum, A.E., White, A.F., Dong, H., 1998. Chemical weathering in a tropical watershed, Luquillo Mountains, Puerto Rico: II. Rate and mechanism of biotite weathering. *Geochimica et Cosmochimica Acta* 62, 227–243.
- Omotoso, O., McCarty, D.K., Hillier, S., Kleeberg, R., 2006. Some successful approaches to quantitative mineral analysis as revealed by the 3rd Reynolds Cup contest. *Clays and Clay Minerals* 54, 748–760.
- Owen, J.J., Dietrich, W.E., Nishizumi, K., Bellugi, D., Amundson, R., 2008. Boundary condition effects on hillslope form and soil development along a climatic gradient from semiarid to hyperarid in northern Chile. *AGU Fall Meeting Supplement*. H53G – 04.
- Paces, T., 1983. Rate constants of dissolution derived from the measurements of mass balance in hydrological catchments. *Geochimica et Cosmochimica Acta* 47, 1855–1863.
- Pett-Ridge, J.C., Derry, L.A., Kurtz, A.C., 2009. Sr isotopes as a tracer of weathering processes and dust inputs in a tropical granitoid watershed, Luquillo Mountains, Puerto Rico. *Geochimica et Cosmochimica Acta* 73, 25–43.
- Price, J.R., Velbel, M.A., Patino, L.C., 2005. Rates and time scales of clay-mineral formation by weathering in saprolitic regoliths of the southern Appalachians from geochemical mass balance. *Geological Society of America Bulletin* 117, 783–794.
- Prospero, J.M., Lamb, P.J., 2003. African droughts and dust transport to the Caribbean: climate change implications. *Science* 302, 1024–1027.
- Prospero, J.M., Bonatti, E., Schubert, C., Carlson, T.N., 1970. Dust in the Caribbean atmosphere traced to an African dust storm. *Earth and Planetary Science Letters* 9, 287–293.
- Prospero, J.M., Glaccum, R.A., Nees, R.T., 1981. Atmospheric transport of soil dust from Africa to South America. *Nature* 289, 570–572.
- Reid, E.A., Reid, J.S., Meier, M.M., Dunlap, M.R., Cliff, S.S., Broumas, A., Perry, K., Maring, H., 2003. Characterization of African dust transported to Puerto Rico by individual particle and size segregated bulk analysis. *Journal of Geophysical Research* 108.
- Riebe, C.S., Kirchner, J.W., Granger, D.E., 2001a. Quantifying quartz enrichment and its consequences for cosmogenic measurements of erosion rates from alluvial sediment and regolith. *Geomorphology* 40, 15–19.
- Riebe, C.S., Kirchner, J.W., Granger, D.E., Finkel, R.C., 2001b. Strong tectonic and weak climatic control of long-term chemical weathering rates. *Geology* 29, 511–514.
- Riebe, C.S., Kirchner, J.W., Finkel, R.C., 2003. Long-term rates of chemical weathering and physical erosion from cosmogenic nuclides and geochemical mass balance. *Geochimica et Cosmochimica Acta* 67, 4411–4427.
- Riebe, C.S., Kirchner, J.W., Finkel, R.C., 2004a. Erosional and climatic effects on long-term chemical weathering rates in granitic landscapes spanning diverse climate regimes. *Earth and Planetary Science Letters* 224, 547–562.
- Riebe, C.S., Kirchner, J.W., Finkel, R.C., 2004b. Sharp decrease in long-term chemical weathering rates along an altitudinal transect. *Earth and Planetary Science Letters* 218, 421–434.
- Schildgen, T.F., Phillips, W.M., Purves, R.S., 2005. Simulation of snow shielding corrections for cosmogenic nuclide surface exposure studies. *Geomorphology* 64, 67–85.
- Schulz, M.S., White, A.F., 1999. Chemical weathering in a tropical watershed, Luquillo Mountains, Puerto Rico III: quartz dissolution rates. *Geochimica et Cosmochimica Acta* 63, 337–350.
- Seiders, V.M., 1971. Geologic map of the El Yunque quadrangle, Puerto Rico, Map I-658. U.S. Geological Survey.
- Small, E.E., Anderson, R.S., Hancock, G.S., 1999. Estimates of the rate of regolith production using ^{10}Be and ^{26}Al from an alpine hillslope. *Geomorphology* 27, 131–150.
- Stallard, R.F., 1985. River chemistry, geology, geomorphology, and soils in the Amazon and Orinoco basins. In: Drever, J.I. (Ed.), *The Chemistry of Weathering*. Springer, pp. 293–316.
- Stone, J.O., 2000. Air pressure and cosmogenic isotope production. *Journal of Geophysical Research* 105, 23753–23759.
- Stonestrom, D.A., White, A.F., Akstin, K.C., 1998. Determining rates of chemical weathering in soils — solute transport versus profile evolution. *Journal of Hydrology* 209, 331–345.
- Swoboda-Colberg, N.G., Drever, J.I., 1993. Mineral dissolution rates in plot-scale field and laboratory experiments. *Chemical Geology* 105, 51–69.
- Taylor, A.B., Velbel, M.A., 1991. Geochemical mass balances and weathering rates in forested watersheds of the southern Blue Ridge II. Effects of botanical uptake terms. *Geoderma* 51, 29–50.
- Turner, B.F., Stallard, R.F., Brantley, S.L., 2003. Investigation of in situ weathering of quartz diorite bedrock in the Rio Icacos basin, Luquillo Experimental Forest, Puerto Rico. *Chemical Geology* 202, 313–341.
- Velbel, M.A., 1985. Geochemical mass balances and weathering rates in forested watersheds of the southern Blue Ridge. *American Journal of Science* 285, 904–930.
- von Blanckenburg, F., Hewawasam, T., Kubik, P.W., 2004. Cosmogenic nuclide evidence for low weathering and denudation in the wet, tropical highlands of Sri Lanka. *Journal of Geophysical Research* 109, F03008.
- Walker, J.C.G., Hays, P.B., Kasting, J.F., 1981. A negative feedback mechanism for the long-term stabilization of Earth's surface temperature. *Journal of Geophysical Research-Oceans and Atmospheres* 86, 9776–9782.
- White, A.F., 2002. Determining mineral weathering rates based on solid and solute weathering gradients and velocities: application to biotite weathering in saprolites. *Chemical Geology* 190, 69–89.
- White, A.F., 2003. Natural weathering rates of silicate minerals. In: Drever, J.I. (Ed.), *Treatise in Geochemistry*, 5. Elsevier, pp. 133–169.
- White, A.F., Brantley, S.L., 2003. The effect of time on the weathering of silicate minerals: why do weathering rates differ in the laboratory and field? *Chemical Geology* 202, 479–506.
- White, A.F., Blum, A.E., Schulz, M.S., Bullen, T.D., Harden, J.W., Peterson, M.L., 1996. Chemical weathering rates of a soil chronosequence on granitic alluvium: I. Quantification of mineralogical and surface area changes and calculation of primary silicate reaction rates. *Geochimica et Cosmochimica Acta* 60, 2533–2550.
- White, A.F., Blum, A.E., Schulz, M.S., Vivit, D.V., Stonestrom, D.A., Larsen, M., Murphy, S.F., Eberl, D., 1998. Chemical weathering in a tropical watershed, Luquillo Mountains, Puerto Rico: I. Long-term versus short-term weathering fluxes. *Geochimica et Cosmochimica Acta* 62, 209–226.
- White, A.F., Schulz, M.S., Vivit, D.V., Blum, A.E., Stonestrom, D.A., Harden, J.W., 2005. Chemical weathering of a soil chronosequence on granitic alluvium: III. Hydrochemical evolution and contemporary solute fluxes and rates. *Geochimica et Cosmochimica Acta* 69, 1975–1996.
- White, A.F., Schulz, M.S., Stonestrom, D.A., Vivit, D.V., Fitzpatrick, J., Bullen, T., 2008. Solute profiles in soils, weathering gradients and exchange equilibrium/disequilibrium. *Mineralogical Magazine* 72, 149–153.
- Yoo, K., Mudd, S.M., 2008. Toward process-based modeling of geochemical soil formation across diverse landforms: a new mathematical framework. *Geoderma* 146, 248–260.
- Yoo, K., Amundson, R., Heimsath, A.M., Dietrich, W.E., Brimhall, G.H., 2007. Integration of geochemical mass balance with sediment transport to calculate rates of soil chemical weathering and transport on hillslopes. *Journal of Geophysical Research* 112, F02013.
- Yoo, K., Mudd, S.M., Sanderman, J., Amundson, R., Blum, A., 2009. Spatial patterns and controls of soil chemical weathering rates along a transient hillslope. *Earth and Planetary Science Letters* 288, 184–193.

Supplementary File

Ferrier K.L., Kirchner J.W., Riebe C.S., and Finkel R.C.

Mineral-specific chemical weathering rates over millennial timescales: Measurements at Rio Icacos, Puerto Rico

As described in the main text, we determined mineral abundances in rock, saprolite and soil samples by processing each sample's XRD pattern in FULLPAT (Chipera and Bish, 2002), a full-pattern inversion method. The average mineral abundances in the bulk rock, saprolite, and soil at sites RI-1 and RI-4 are recorded in Tables 3 and 4, and we present in Table SF2 all of the sample mineral abundances from which the average abundances were derived. These abundances were converted to units of mol kg⁻¹ with the molar masses in Table SF1.

In Figures SF1 and SF2, locations of all samples are mapped on subsections of the El Yunque USGS topographic quadrangle (USGS, 1982), and show the range of locations from which soil, rock, and saprolite samples were collected in the study catchments.

Table SF1: Mineral molar masses (after White et al., 1998)

Mineral	Formula	Molar mass (g mol ⁻¹)
Quartz	SiO ₂	60.08
Plagioclase	Na _{0.60} Ca _{0.40} Al _{1.36} Si _{2.63} O ₈	268.38
Hornblende	(Na _{0.34} K _{0.05})(Ca _{1.71} Mg _{2.84} Fe _{2.06} Al _{0.89})(Al _{1.00} Si _{6.68})O ₂₂ (OH) ₂	886.98
Biotite	K _{0.85} (Al _{0.10} Ti _{0.20} Fe _{1.35} Mg _{1.25})(Si _{2.8} Al _{1.2})O ₁₀ (OH) ₂	456.30
Kaolinite	Al ₂ Si ₂ O ₅ (OH) ₄	258.16

Table SF2: Sample mineral abundances (weight percent)

RI-1 soils			Mineral abundances (%)			
Sample	Depth (cm)	Slope (%)	Quartz	Plagioclase	Hornblende	Biotite
RI-1P1B	33	n.d.	57.1	0.0	0.9	0.0
RI-1P2B	42	n.d.	60.7	0.0	2.0	0.0
RI-1P3B	55	51	34.7	0.0	0.0	0.0
RI-1P3BC	92	51	25.6	0.0	1.6	0.0
RI-1P4B1	25	58	62.3	4.1	3.3	0.0
RI-1P4B2	50	58	43.0	0.0	2.2	0.0
RI-1P5A	8	31	50.8	0.0	0.0	0.0
RI-1P5B	25	31	47.9	0.0	0.0	0.0
RI-1P6B	21	45	50.8	3.2	11.2	0.0
RI-1P7A	11	70	45.1	4.9	4.7	0.0
RI-1P7B	37	70	52.6	3.4	5.0	0.0
RI-1P8A	6	35	48.1	0.0	0.0	0.0
RI-1P8B	32	35	51.6	0.0	0.0	0.0
mean ± s.e.			48.5 ± 2.8	1.2 ± 0.5	2.4 ± 0.9	0.0 ± 0.0

RI-1 rocks			Mineral abundances (%)			
Sample	Depth (cm)	Slope (%)	Quartz	Plagioclase	Hornblende	Biotite
RI-1X1	surface	n.d.	24.5	56.7	13.6	0.6
RI-1X2	surface	n.d.	28.2	61.6	12.4	0.6
RI-1X3	surface	n.d.	26.2	57.4	10.5	0.2
RI-1X4	surface	n.d.	23.9	51.8	12.8	0.4
RI-1X5	surface	n.d.	25.2	53.4	10.1	0.6
RI-1P4X	surface	n.d.	7.7	n.d.	n.d.	0.1
mean ± s.e.			22.6 ± 3.0	56.2 ± 1.7	11.9 ± 0.7	0.4 ± 0.1

RI-4 saprolite			Mineral abundances (%)			
Sample	Depth (cm)	Slope (%)	Quartz	Plagioclase	Hornblende	Biotite
RI-4P9S (28)	95-117	25	27.8	0.0	0.0	0.0
RI-4P9S (29)	117-135	25	24.3	0.0	0.0	0.0
RI-4P9S (30)	135-150	25	24.9	0.0	0.0	0.0
RI-4P9S (31)	150-168	25	24.1	0.0	0.0	0.0
RI-4P9S (32)	168-187	25	24.1	0.0	0.0	0.0
RI-4P9S (33)	187-203	25	26.6	0.0	0.0	0.0
RI-4P9S (34)	203-219	25	27.6	0.0	0.0	0.0
RI-4S1	road cut	n.d.	28.1	0.0	0.0	0.0
RI-4S2	road cut	n.d.	21.4	15.5	20.4	0.0
RI-4P10S (45)	143-156	60	24.8	0.0	0.0	0.0
RI-4P10S (46)	180-196	60	26.2	0.0	0.0	0.0
RI-4P10S (47)	196-209	60	24.9	0.0	0.0	0.0
RI-4P10S (48)	209-222	60	27.5	0.0	0.0	0.0
mean ± s.e.			25.6 ± 0.5	1.2 ± 1.2	1.6 ± 1.6	0.0 ± 0.0

RI-4 soils			Mineral abundances (%)			
Sample	Depth (cm)	Slope (%)	Quartz	Plagioclase	Hornblende	Biotite
RI-4P1A	5	54	48.0	0.0	0.9	0.0
RI-4P1B	34	54	48.6	0.0	0.0	0.0
RI-4P2A	9	74	59.6	5.7	4.1	0.0
RI-4P2B1	29	74	56.3	4.1	5.4	0.0
RI-4P2B2	48	74	56.2	5.1	4.1	0.0
RI-4P3W1	root wad	n.d.	41.5	9.8	11.1	0.0
RI-4P3W2	root wad	n.d.	43.7	8.6	7.5	0.0
RI-4P4A	3	71	66.3	6.3	6.3	0.0
RI-4P4B1	16	71	63.6	7.0	5.3	0.0
RI-4P4B2	33	71	62.6	6.1	5.8	0.0
RI-4P5W1	root wad	56	82.7	0.0	1.7	0.0
RI-4P5W2	root wad	56	76.7	0.0	0.0	0.0
RI-4P6W1	root wad	32	45.1	0.0	0.0	0.0
RI-4P6W2	root wad	32	47.2	0.0	0.0	0.0
RI-4P7B	8-37	86	33.3	4.3	10.6	0.0
RI-4P8A	20	54	58.8	0.0	2.3	0.0
RI-4P8B1	27	54	63.7	0.0	1.8	0.0
RI-4P8B2	44	54	61.5	0.0	2.5	0.0
RI-4P8W1	root wad	54	70.4	0.0	3.1	0.0
RI-4P8W2	root wad	54	58.5	0.0	2.9	0.0
RI-4P9AB1	0-27	25	52.9	0.0	0.0	0.0
RI-4P9B2	27-44	25	62.4	0.0	0.0	0.0
RI-4P9B3	44-62	25	64.0	0.0	0.0	0.0
RI-4P9B4 (26)	62-76	25	51.7	0.0	0.0	0.0
RI-4P9B4 (27)	76-95	25	31.7	0.0	0.0	0.0
RI-4P10A	0-26	60	71.1	0.0	0.0	0.0
RI-4P10B1	39-55	60	67.4	0.0	0.0	0.0
RI-4P10B2 (38)	55-70	60	70.0	0.0	0.0	0.0
RI-4P10B2 (40)	81-91	60	56.7	0.0	0.0	0.0
RI-4P10B3	103-116	60	34.9	0.0	0.0	0.0
mean ± s.e.			56.9 ± 2.3	1.9 ± 0.6	2.5 ± 0.6	0.0 ± 0.0

RI-4 rocks			Mineral abundances (%)			
Sample	Depth (cm)	Slope (%)	Quartz	Plagioclase	Hornblende	Biotite
RI-4X1	surface	n.d.	22.4	51.9	12.7	0.3
RI-4X2	surface	n.d.	24.1	57.7	13.8	0.5
RI-4X3	surface	n.d.	19.3	58.4	22.4	0.8
RI-4X4	surface	n.d.	23.8	n.d.	23.8	1.1
RI-4X5	surface	n.d.	19.3	n.d.	24.5	1.5
mean ± s.e.			21.8 ± 1.1	56.0 ± 2.1	19.4 ± 2.6	0.8 ± 0.2

In Table SF2, some of the sample depths are designated as “root wad”, which denotes opportunistic samples of the subsurface, collected from root wads of freshly downed trees. Samples S1 and S2 in RI-4 were collected from saprolite exposed in a road cut.

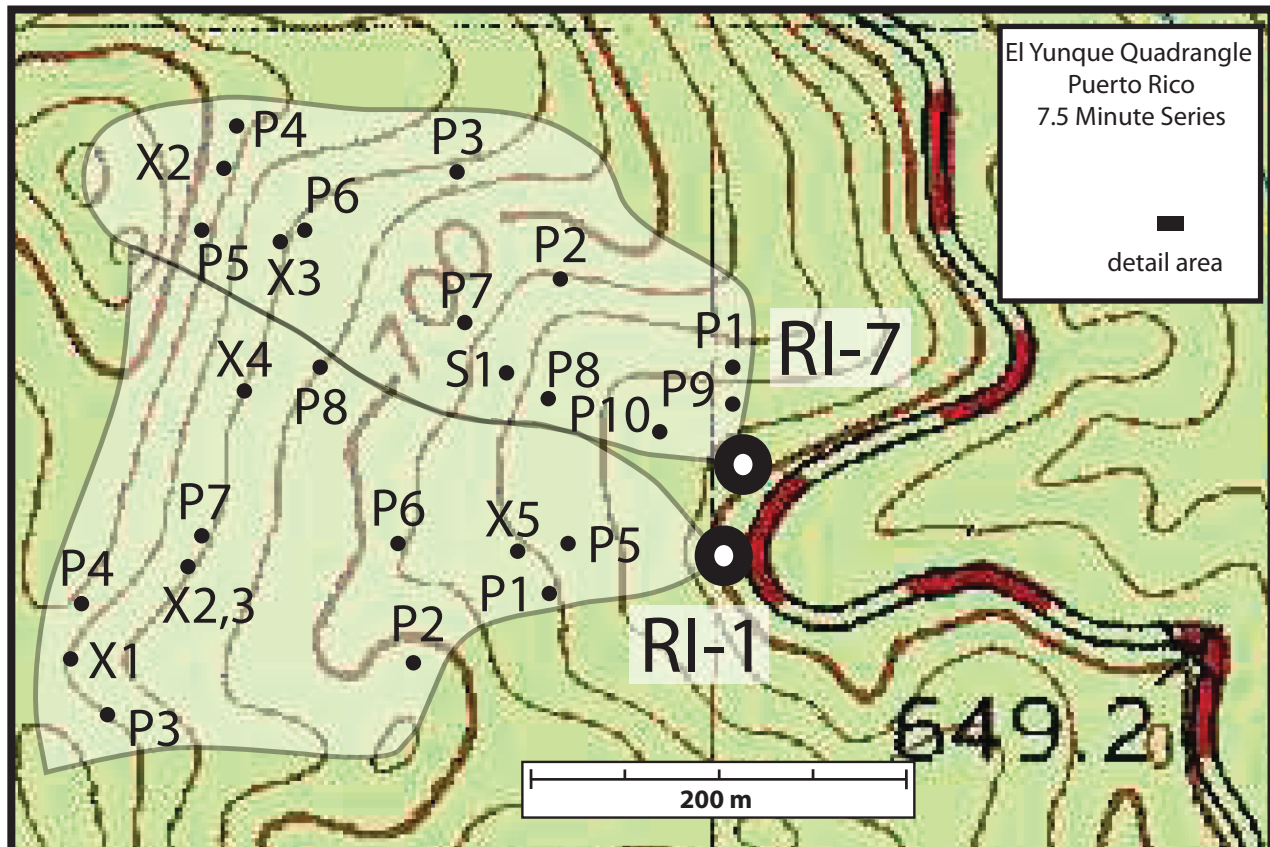


Figure SF1. Rio Icacos sampling sites "RI-1" and "RI-7" from Riebe et al. (2003), showing locations of soil pits (with prefix = "P"), rocks (with prefix = "X"), and exposed saprolite (with prefix = "S") deduced in the field from line of sight and dead reckoning using a compass and altimeter.

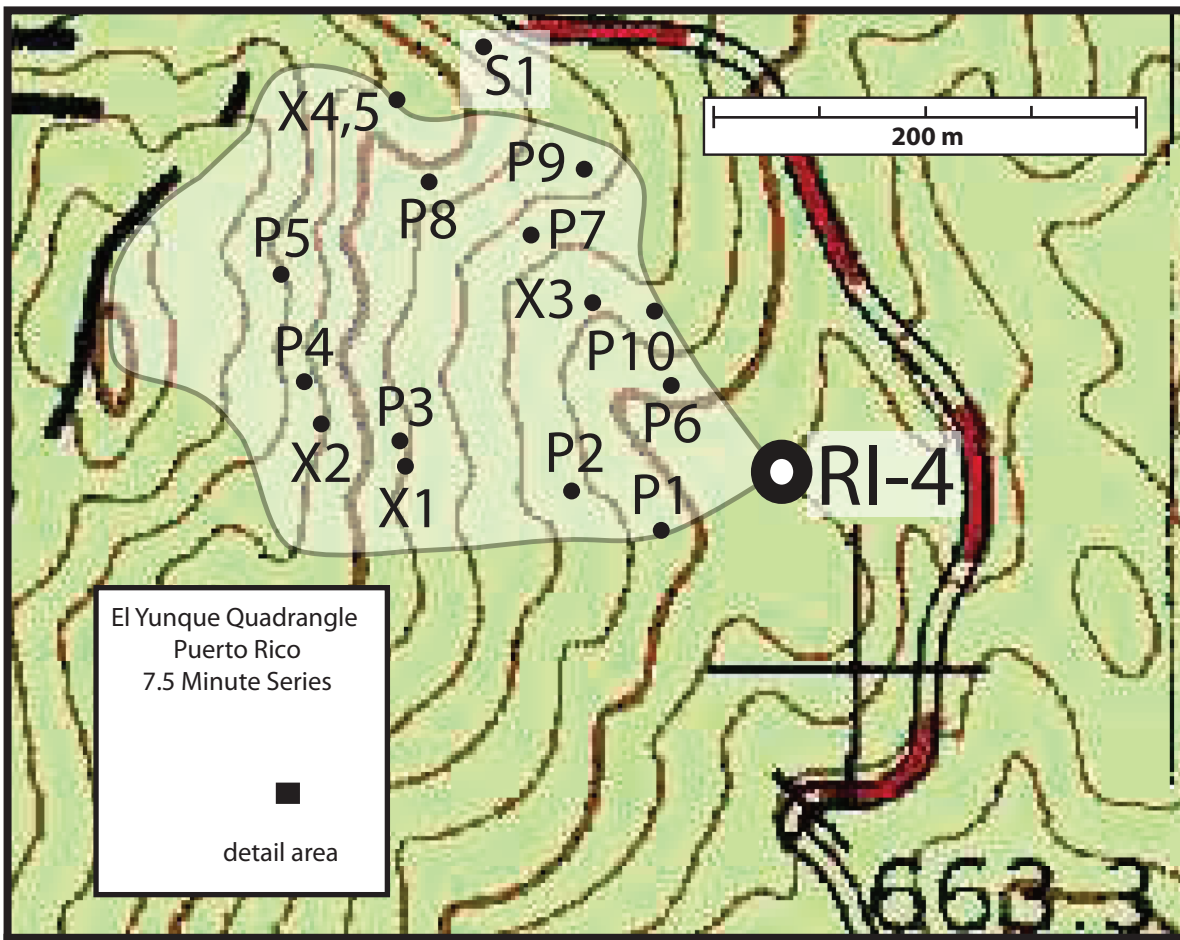


Figure SF2. Rio Icacos sampling site "RI-4" from Riebe et al. (2003) showing locations of soil pits (with prefix = "P"), rocks (with prefix = "X"), and exposed saprolite (with prefix = "S") deduced in the field from line of sight and dead reckoning using a compass and altimeter. P9 and P10 were sampled with an auger.

References

- Chipera S.J., Bish D.L., 2002. FULLPAT: a full-pattern quantitative analysis program for X-ray powder diffraction using measured and calculated patterns. *Journal of Applied Crystallography*, v. 35, p. 744-749.
- USGS, 1982. El Yunque Quadrangle, Puerto Rico, 7.5 Minute Series. U.S. Geological Survey, Reston, VA.